

Endothelial TWIK-related potassium channel-1 (TREK1) regulates immune-cell trafficking into the CNS

Stefan Bittner^{1,8}, Tobias Ruck^{1,8}, Michael K Schuhmann^{1,2}, Alexander M Herrmann¹, Hamid Moha ou Maati³, Nicole Bobak¹, Kerstin Göbel¹, Friederike Langhauser², David Stegner^{2,4}, Petra Ehling^{1,5}, Marc Borsotto³, Hans-Christian Pape⁶, Bernhard Nieswandt⁴, Christoph Kleinschnitz², Catherine Heurteaux³, Hans-Joachim Galla⁷, Thomas Budde⁶, Heinz Wiendl^{1,8} & Sven G Meuth^{1,5,8}

The blood-brain barrier (BBB) is an integral part of the neurovascular unit (NVU). The NVU is comprised of endothelial cells that are interconnected by tight junctions resting on a parenchymal basement membrane ensheathed by pericytes, smooth muscle cells and a layer of astrocyte end feet¹. Circulating blood cells, such as leukocytes, complete the NVU². BBB disruption is common in several neurological diseases, but the molecular mechanisms involved remain largely unknown³. We analyzed the role of TWIK-related potassium channel-1 (TREK1, encoded by *KCNK2*) in human and mouse endothelial cells and the BBB. TREK1 was downregulated in endothelial cells by treatment with interferon- γ (IFN- γ) and tumor necrosis factor- α (TNF- α). Blocking TREK1 increased leukocyte transmigration, whereas TREK1 activation had the opposite effect. We identified altered mitogen-activated protein (MAP) kinase signaling, actin remodeling and upregulation of cellular adhesion molecules as potential mechanisms of increased migration in TREK1-deficient (*Kcnk2*^{-/-}) cells. In *Kcnk2*^{-/-} mice, brain endothelial cells showed an upregulation of the cellular adhesion molecules ICAM1, VCAM1 and PECAM1 and facilitated leukocyte trafficking into the CNS. Following the induction of experimental autoimmune encephalomyelitis (EAE) by immunization with a myelin oligodendrocyte protein (MOG)_{35–55} peptide, *Kcnk2*^{-/-} mice showed higher EAE severity scores that were accompanied by increased cellular infiltrates in the central nervous system (CNS). The severity of EAE was attenuated in mice given the amyotrophic lateral sclerosis drug riluzole or fed a diet enriched with linseed oil (which contains the TREK-1 activating omega-3 fatty acid α -linolenic acid). These beneficial effects were reduced in *Kcnk2*^{-/-} mice, suggesting TREK-1 activating compounds may be used therapeutically to treat diseases related to BBB dysfunction.

Dysfunction of the BBB is a pathologic feature that is common to several neurological disorders³. The molecular mechanisms underlying BBB dysfunction remain unclear. Ion channels have gained attention as potential pharmaceutical targets in neurologic diseases⁴. TREK1 is a member of the two-pore domain potassium (K_{2P}) channel family⁵. It is modulated by various stimuli, such as membrane stretch, heat and cellular lipids (for example, polyunsaturated fatty acids (PUFAs))⁵. Recent evidence suggests that neuronal TREK1 has a role in depression⁶, pain⁷ and neuroprotection⁸.

We investigated the role of TREK1 in CNS barrier function. Western blot analysis showed that wild-type (WT) primary mouse brain microvascular endothelial cells (MBMECs) express TREK1 (Fig. 1a) but no other K_{2P} channel proteins, for example, TREK2 (also known as KCNK10), TRAAK (also known as KCNK4), TRESK (also known as KCNK18) or TASK1–TASK3 (also known as KCNK3, KCNK5 and KCNK9, respectively) (data not shown). The TREK1-specific antagonist spadin⁹ decreased outward currents of single WT MBMECs. *Kcnk2*^{-/-} MBMECs showed reduced outward rectification but were insensitive to spadin (Fig. 1b). Detailed analyses of the electrophysiological effects of various TREK1-modulating agents are shown in Supplementary Figure 1a–f.

We investigated whether TREK1 activity affects MBMEC barrier properties. Although transendothelial resistance (TER) was unaltered in *Kcnk2*^{-/-} MBMECs compared to WT cells (Fig. 1c), trafficking of CD4⁺ lymphocytes was significantly higher across *Kcnk2*^{-/-} MBMEC monolayers regardless of whether the lymphocytes were collected from WT or *Kcnk2*^{-/-} mice (Fig. 1d). Incubation of cocultured cells with spadin resulted in a comparable increase in migration of WT CD4⁺ T cells across WT but not *Kcnk2*^{-/-} MBMEC monolayers (Fig. 1d). We obtained similar results for CD8⁺ T cells (data not shown). *Kcnk2* knockout status did not alter the growth density of MBMECs (Supplementary Fig. 2a). We did not detect TREK1 expression in T lymphocytes at either the RNA or protein level (data not shown), and *Kcnk2*^{-/-} and WT splenocytes did not differ with respect

¹Department of Neurology, University of Münster, Münster, Germany. ²Department of Neurology, University of Würzburg, Würzburg, Germany. ³Institut de Pharmacologie Moléculaire et Cellulaire, Centre National de la Recherche Scientifique (CNRS), Université de Nice Sophia Antipolis, Valbonne, France. ⁴Chair of Vascular Medicine, University Hospital Würzburg and Rudolf Virchow Center, Deutsche Forschungsgemeinschaft Research Center for Experimental Biomedicine, University of Würzburg, Würzburg, Germany. ⁵Institute of Physiology I–Neuropathophysiology, University of Münster, Münster, Germany. ⁶Institute of Physiology I, University of Münster, Münster, Germany. ⁷Institute of Biochemistry, University of Münster, Münster, Germany. ⁸These authors contributed equally to this work. Correspondence should be addressed to S.B. (stefan.bittner@ukmuenster.de) or S.G.M. (sven.meuth@ukmuenster.de).

Received 21 March; accepted 16 July; published online 11 August 2013; doi:10.1038/nm.3303

Figure 1 TREK1 inhibition or deletion

facilitates lymphocyte migration into the CNS and worsens autoimmune CNS inflammation.

(a) TREK1 protein expression in MBMECs from WT and *Kcnk2*^{-/-} mice (*n* = 5 mice per group, one representative western blot including β -actin as the loading control is shown).

(b) Electrophysiological measurement of membrane currents of single MBMECs from WT and *Kcnk2*^{-/-} mice in the presence or absence of the TREK1 inhibitor spadin (1 μ M).

Left, representative current examples. Right, the change in current (Δ Current) after spadin treatment compared to control conditions (*n* = 5 cells per group).

(c) The TER of WT and *Kcnk2*^{-/-} MBMECs over 7 d (*n* = 5 wells per group). The smaller graphs above show the parallel measured capacitance of the cell layer (C_{CL}) and the effect of hydrocortisone (HC) on the TER as a positive control. The dotted box indicates the time frame when cells were confluent.

(d) Migration (expressed as the cell:bead ratio) of WT CD4⁺ T cells across a WT or *Kcnk2*^{-/-} MBMEC monolayer in the presence or absence of spadin (2 μ M). The groups shown are as follows (denoted as the genotype of the MBMECs/the genotype of the lymphocytes/spadin treatment): A, WT/WT/no; B, knockout/WT/no; C, WT/WT/yes; D, WT/knockout/no; E, knockout/knockout/no; F, knockout/knockout/yes. *n* = 6 wells per group.

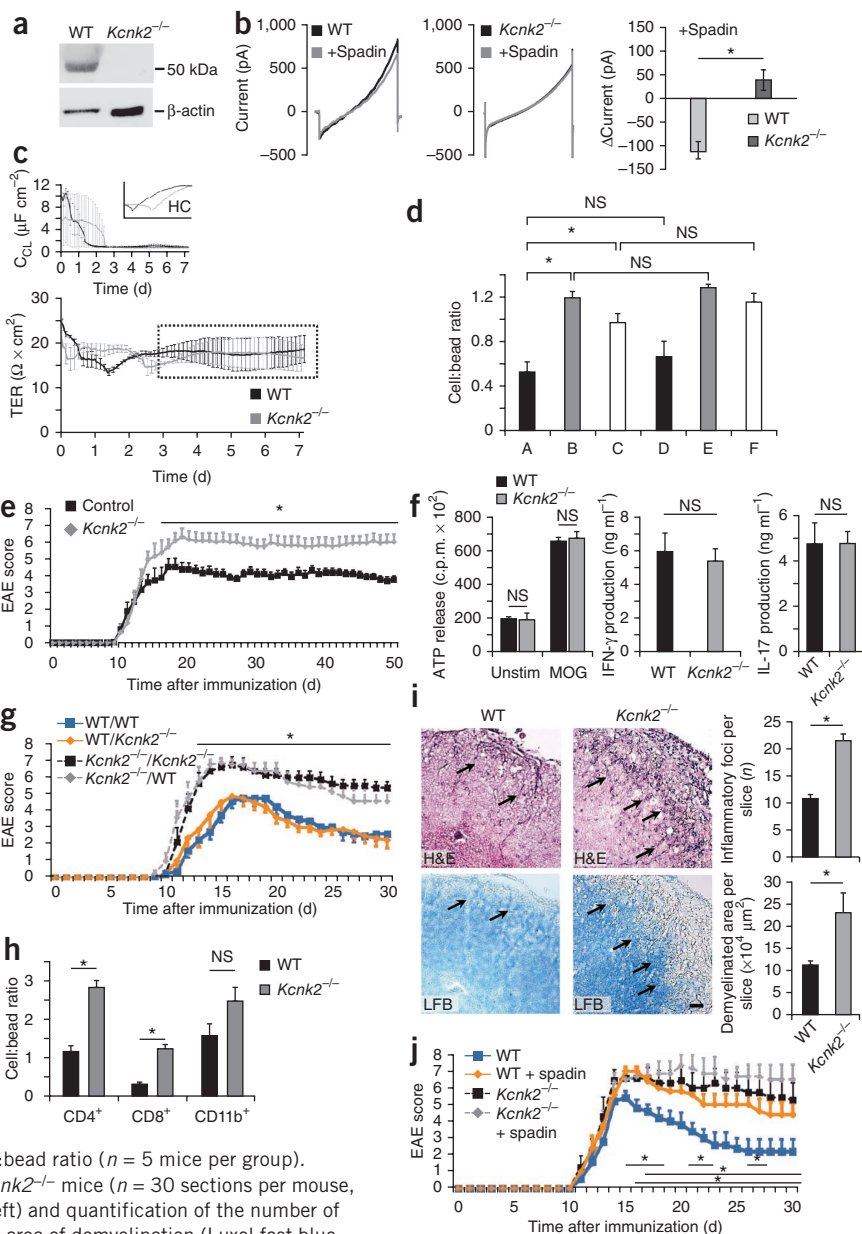
(e) EAE disease scores in WT and *Kcnk2*^{-/-} mice (*n* = 15 mice per group). (f) Proliferation assays and ELISAs for IFN- γ and IL-17 production (*n* = 5 mice per group) in WT and *Kcnk2*^{-/-} splenocytes isolated from mice at the maximum point of disease. Unstim, unstimulated.

(g) EAE disease scores in reciprocal bone marrow chimeras of WT and *Kcnk2*^{-/-} mice (*n* = 8–9 per group). The legend shows the genotype of the recipient/the genotype of the bone marrow.

(h) Flow cytometric quantification of different immune cell subsets (CD4⁺, CD8⁺ lymphocytes and CD11b⁺ macrophages and microglia) isolated from the spinal cord of WT or *Kcnk2*^{-/-} mice after EAE (at disease maximum) expressed as the cell:bead ratio (*n* = 5 mice per group).

(i) Representative staining of spinal cords of WT or *Kcnk2*^{-/-} mice (*n* = 30 sections per mouse, *n* = 5 mice per group) at the maximum point of EAE (left) and quantification of the number of inflammatory foci (H&E staining, black arrows) and the area of demyelination (Luxol fast blue (LFB) staining, black arrows) (right). Scale bar, 10 μ m.

(j) Effect of spadin (100 μ M, 10 μ M daily intraperitoneally (i.p.)) on the course of EAE in WT and *Kcnk2*^{-/-} mice (*n* = 10–12 mice per group). Significant differences between the EAE scores are indicated (upper lines, WT compared to WT + spadin; middle line, WT compared to *Kcnk2*^{-/-}; lower line, WT compared to *Kcnk2*^{-/-} + spadin). All data are shown as the mean \pm s.e.m. **P* < 0.05, determined by Student's *t* test (b,i), analysis of variance (ANOVA) (d,g,j) or Mann-Whitney test (e,f,h). NS, not significant.



to cytokine production (Supplementary Fig. 2b), proliferation (Supplementary Fig. 2c) or migration across transwell filters (Supplementary Fig. 2d).

We then assessed the effect of TREK1 on BBB function using a well-established mouse model of inflammation-related BBB dysfunction, MOG peptide-induced EAE. *Kcnk2*^{-/-} mice had higher EAE clinical scores starting at day 18 after immunization (Fig. 1e). *Kcnk2*^{-/-} and WT splenocytes isolated from mice at the peak of disease (day 18) showed no differences in terms of proliferation and production of IFN- γ and interleukin-17 (IL-17) after re-stimulation (Fig. 1f). We generated bone marrow chimeras by transferring WT and *Kcnk2*^{-/-} bone marrow cells into irradiated WT and *Kcnk2*^{-/-} recipients. After the induction of EAE in these mice, WT recipients of WT or *Kcnk2*^{-/-} bone marrow developed similar disease, whereas *Kcnk2*^{-/-} recipients

of either type of bone marrow had higher disease scores, suggesting that TREK1 deficiency in radioresistant cells exacerbates disease (Fig. 1g). We observed similar results in adoptive-transfer EAE experiments in WT recipients using MOG_{35–55}-specific cells from 2D2 or 2D2 \times *Kcnk2*^{-/-} mice (Supplementary Fig. 2e). Coculture experiments of dendritic cells (DCs) and T cells from immunized WT and *Kcnk2*^{-/-} mice revealed no significant differences in the amount of IFN- γ in the culture medium (Supplementary Fig. 2f). DCs from *Kcnk2*^{-/-} and WT mice showed no differences in the expression of co-stimulatory molecules or activation markers (Supplementary Fig. 2g). In *Kcnk2*^{-/-} mice, increased numbers of CD4⁺ and CD8⁺ T cells infiltrated the CNS as compared to WT mice when we examined the mice at day 18 (Fig. 1h). Immunohistochemistry revealed significantly higher numbers of inflammatory foci and enlarged areas of demyelination in the absence

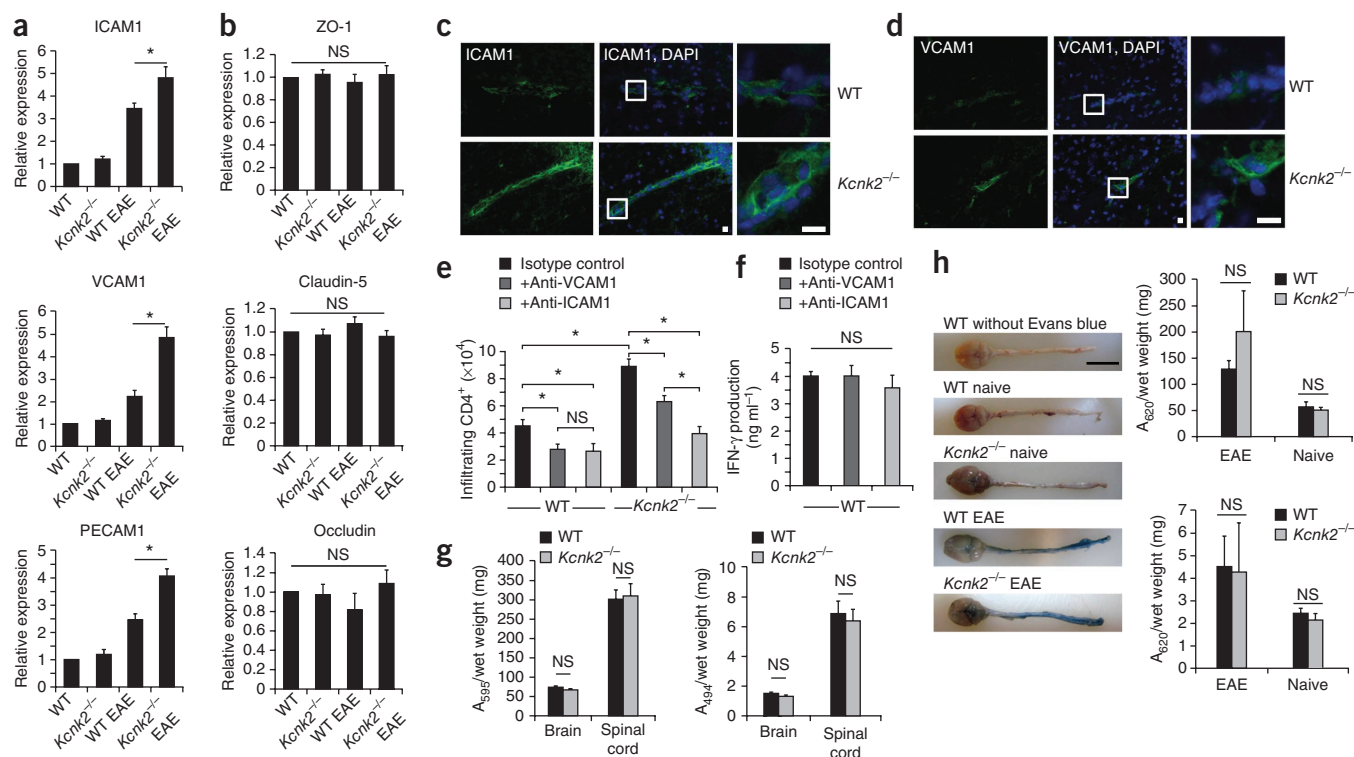


Figure 2 TREK1 deficiency leads to upregulation of cellular adhesion molecules and enhances immune-cell infiltration into the CNS *in vivo*. (a,b) RT-PCR analysis of the relative gene expression of cellular adhesion molecules (a) and TJPs (b) in MBMECs isolated from naive WT and *Kcnk2*^{-/-} mice or from WT and *Kcnk2*^{-/-} mice at EAE disease maximum normalized to naive WT MBMECs (*n* = 5 mice per group). (c,d) Representative immunohistochemical staining for ICAM1 and VCAM1 in EAE lesions of WT and *Kcnk2*^{-/-} mice. The images on the far right are higher magnifications of the boxed areas. Scale bars, 10 μ m. (e) Number of CNS-infiltrating CD4⁺ T lymphocytes in WT and *Kcnk2*^{-/-} mice receiving blocking antibodies to VCAM1 or ICAM1 at days 8 and 9 (Online Methods) (*n* = 5 mice per group). (f) IFN- γ production from isotype control-treated or antibody-treated WT splenocytes at disease maximum (Online Methods) as assessed by ELISA. (g) Quantification of Texas red-dextran (70 kDa; left) and fluorescein-dextran (3 kDa; right) extravasation into the CNS 1 h after intravenous application in immunized mice at day 18, as assessed by absorbance at 595 nm (*A*₅₉₅) and 494 nm (*A*₄₉₄) (*n* = 5 mice per group). No significant difference was observed in naive mice (data not shown). (h) Extravasation of Evans blue into the CNS 24 h after intravenous injection. Left, representative images from control mice (WT without Evans blue), naive and EAE mice. Right, quantification of the results for the brain and spinal cord (*n* = 5 mice per group). Scale bar, 1 cm. All data are shown as the mean \pm s.e.m. **P* < 0.05, determined by Mann-Whitney test (a,b,g-i) or ANOVA (e,f). NS, not significant.

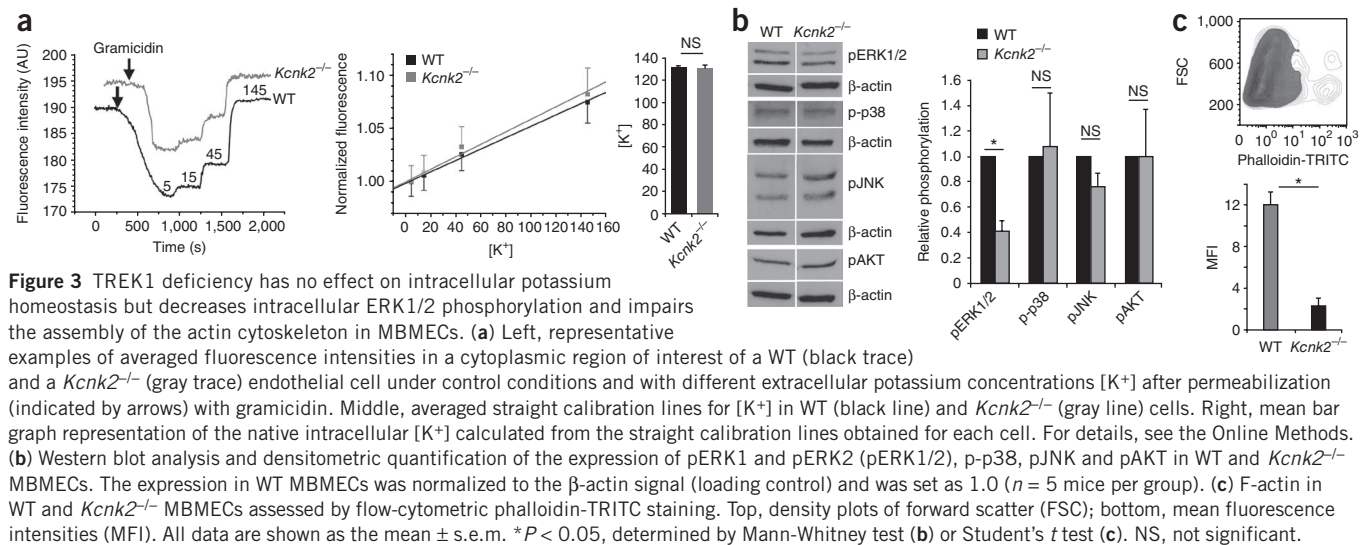
of TREK1 (Fig. 1i). Spadin significantly worsened the course of EAE in WT mice but not in immunized *Kcnk2*^{-/-} mice (Fig. 1j).

To investigate the mechanisms underlying increased trafficking of lymphocytes in TREK1-deficient mice, we examined cellular adhesion molecules. Expression of intercellular adhesion molecule 1 (ICAM1), vascular cell adhesion molecule 1 (VCAM1) and platelet endothelial cell adhesion molecule 1 (PECAM1) mRNA were all significantly higher in *Kcnk2*^{-/-} than WT MBMECs following the induction of EAE but not under noninflammatory conditions (Fig. 2a). The expression of tight-junction proteins (TJPs) remained unchanged (Fig. 2b). Immunohistochemistry confirmed these results at the protein level (Fig. 2c,d and Supplementary Fig. 3a–d). We then applied blocking antibodies to VCAM1 and ICAM1 in EAE mice. Administration of these antibodies (see Online Methods) reduced disease scores, and this effect was more pronounced in *Kcnk2*^{-/-} mice (Supplementary Fig. 4a,b). Blockade of VCAM1 reduced the number of CNS-infiltrating CD4⁺ cells in both WT and *Kcnk2*^{-/-} mice to a comparable degree, whereas an ICAM1-blocking antibody had a larger effect in *Kcnk2*^{-/-} mice, arguing for a major role of ICAM1 upregulation (Fig. 2e). We observed no significant changes in IFN- γ production after MOG re-stimulation of splenocytes isolated from antibody-treated mice (Fig. 2f and Supplementary Fig. 4c). BBB permeability *in vivo* to vascular

tracer molecules (Texas red-dextran (70 kDa), fluorescein-dextran (3 kDa) and Evan's blue dye) at the maximum point of EAE did not differ between *Kcnk2*^{-/-} and WT mice (Fig. 2g,h). We corroborated these results *in vitro* in MBMECs (Supplementary Fig. 5a,b).

In potassium-imaging experiments, intracellular K⁺ concentrations ([K⁺]) were unaltered in endothelial cells from *Kcnk2*^{-/-} mice, suggesting that TREK1 deficiency does not affect intracellular [K⁺] (Fig. 3a). Western blot analyses showed that the expression of phosphorylated Erk (pERK), but not other phosphorylated signaling molecules (p-p38, pJNK or pAKT), was reduced in IFN- γ - and TNF- α -treated *Kcnk2*^{-/-} MBMECs compared to WT cells (Fig. 3b), suggesting that loss of TREK1 alters ERK phosphorylation in brain endothelial cells.

Actin cytoskeleton dynamics have a crucial role in modulating leukocyte-endothelial cell interactions¹⁰. Flow cytometry using phalloidin-tetramethylrhodamine isothiocyanate (TRITC) staining showed reduced F-actin content in *Kcnk2*^{-/-} MBMECs (Fig. 3c). Recently, a role for TREK1 in nitric oxide production was suggested, but definitive evidence is pending^{11,12}. We therefore used the nitric oxide synthase inhibitor L-NG-nitroarginine methyl ester (L-NAME)¹¹ in our transwell migration assay *in vitro* but did not observe any impact on BBB function (data not shown). Excessive nitric oxide release can lead to the generation of reactive nitrogen species and free radical formation.

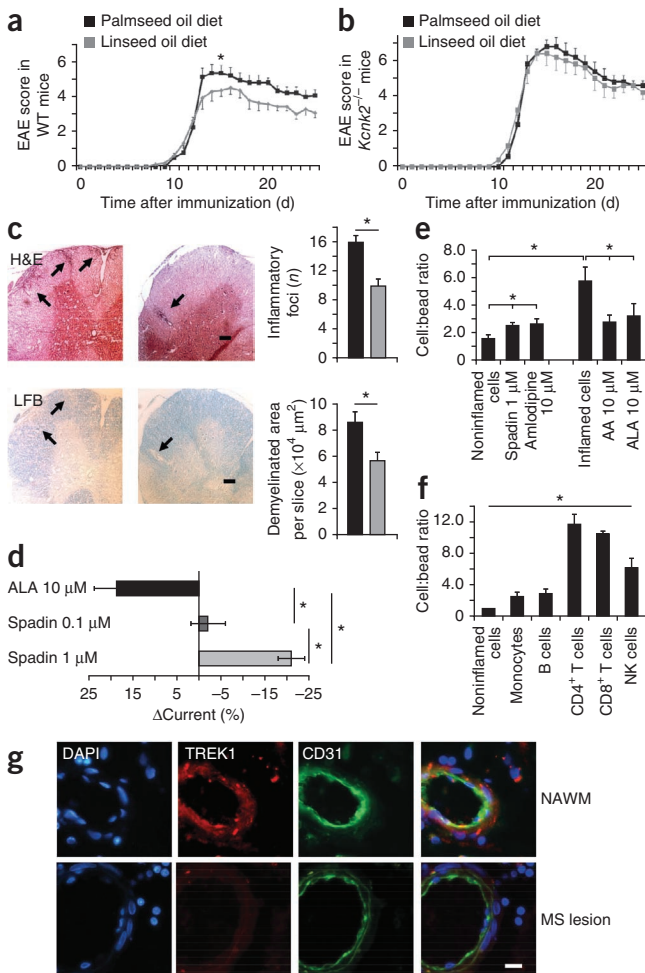


Dihydroethidium (DHE) and nitrotyrosine staining of EAE lesions did not reveal any differences in reactive nitrogen or reactive oxygen formation (Supplementary Fig. 6a,b). We confirmed this observation using sensor dyes for nitric oxide (4-amino-5-methylamino-2', 7'-difluorofluorescein (DAF-FM); data not shown) and for production of reactive oxygen species (ROS) and reactive nitrogen species (CM-H2DCFDA) *in vitro* (Supplementary Fig. 6c). Thus, the

decreased barrier stability observed in *Kcnk2*^{-/-} mice is probably not due to changes in nitric oxide or nitric oxide-related free-radical production. Furthermore, cultured astrocytes from WT and *Kcnk2*^{-/-} mice did not differ significantly with respect to morphology, cytokine production or expression of marker proteins (Supplementary Fig. 7a–c). We found similar numbers of astrocytes in lesions from WT mice and *Kcnk2*^{-/-} mice, and there was no significant difference in astrocyte morphology (Supplementary Fig. 7d,e).

Treatment of WT and *Kcnk2*^{-/-} mice with the TREK1 activator riluzole¹³ substantially attenuated the course of EAE¹⁴ (Supplementary Fig. 8a). This effect was delayed until up to day 15 in *Kcnk2*^{-/-} mice (Supplementary Fig. 8b), suggesting an additional effect of riluzole in EAE that is independent of TREK1. The expression of ICAM1, VCAM1 and PECAM1 mRNA were upregulated and immune cell infiltration in the CNS was reduced in WT mice receiving riluzole compared with untreated controls. However, cell proliferation and cytokine production (IFN-γ and IL-17) of immune cells re-stimulated with MOG peptide did not differ between the two groups (Supplementary Fig. 8c–e).

Figure 4 A linseed oil-rich diet, which activates TREK1, reduces EAE scores, and TREK1 is downregulated in individuals with multiple sclerosis. **(a,b)** EAE disease scores in WT **(a)** and *Kcnk2*^{-/-} **(b)** mice fed a diet enriched with 5% palmseed oil or linseed oil (*n* = 15 mice per group). **(c)** Left, representative histologic staining showing inflammatory foci (H&E, top) and demyelination (LFB, bottom) in the spinal cords (black arrows) of WT mice receiving a diet enriched with palmseed oil (left) or linseed oil (right). Right, quantification of the data in palmseed (black) or linseed (gray) oil-fed mice. Scale bars, 250 μm. **(d)** Effect of ALA (10 μM) or spadin (0.1 or 1 μM) on whole-cell patch-clamp recordings of membrane currents of single HBMECs (n = 4 cells per group). **(e)** Transmigration assay of PBMCs across noninflamed HBMEC cell layers in the presence or absence of the TREK1 inhibitors spadin (1 μM) and amlodipine (10 μM) (left group) and of PBMCs across inflamed HBMEC cell layers in the presence or absence of the TREK1 activators arachidonic acid (AA; 10 μM) and ALA (10 μM) (right group) (*n* = 5 cells per group). **(f)** Relative migration of different immune cells across HBMEC cell layers pretreated with IFN-γ and TNF-α before the migration assays normalized to basal conditions (noninflamed cells, set to a value of 1) (*n* = 5 cells per group). NK, natural killer. **(g)** TREK1 and CD31 (PECAM1) expression in normal-appearing white matter (NAWM) and inflammatory lesions (MS lesion) of subjects with multiple sclerosis. Scale bar, 30 μm. All data are shown as the mean ± s.e.m. **P* < 0.05, determined by Mann-Whitney test (**a**), Student's *t* test (**c**) or ANOVA (**d–f**).



As TREK1-activating PUFAs have beneficial effects on coronary and cerebrovascular diseases^{15–17}, we compared EAE symptoms in mice that received a diet enriched with linseed oil (which contains high amounts of the TREK1-activating omega-3 fatty acid α -linolenic acid (ALA)) or a standard diet enriched with palmseed oil. The severity of EAE was reduced in WT mice fed linseed oil (Fig. 4a) but not in linseed oil-fed *Kcnk2*^{−/−} mice as compared to mice fed a palmseed oil diet (Fig. 4b). Daily food intake, splenocyte proliferation and cytokine production were comparable between WT mice fed the linseed oil diet and those fed the palmseed oil diet (Supplementary Fig. 9a,b). Histologic examination revealed reduced cellular infiltration into the CNS and reduced demyelination in linseed oil-fed mice (Fig. 4c).

To demonstrate the relevance of our findings in humans, we investigated cultured human brain microvascular endothelial cells (HBMECs). We detected expression of TREK1 mRNA by RT-PCR analysis in HBMECs but not any other K₂P channel protein tested (Supplementary Fig. 10a). Consistent with our findings in mice, the expression of TREK1 was reduced after culture with either lipopolysaccharide, IFN- γ , TNF- α or IFN- γ plus TNF- α (Supplementary Fig. 10b,c). Electrophysiological recordings demonstrated that TREK1 activation with ALA increased, whereas TREK1 blockade with spadin decreased, the outward currents of single HBMECs (Fig. 4d). Inhibition of TREK1 with spadin or amlodipine enhanced the transmigration of peripheral blood mononuclear cells (PBMCs) across noninflamed HBMEC layers, whereas TREK1 activation with arachidonic acid or ALA reduced transmigration across inflamed HBMEC layers (Fig. 4e,f and Supplementary Fig. 10d,e). In HBMECs, TREK1 activation with arachidonic acid or ALA reversed the reduction in F-actin content induced by simultaneous treatment with IFN- γ and TNF- α (Supplementary Fig. 11). TREK1 modulation did not affect human endothelial cell production of cytokines and chemokines or the expression of cellular adhesion molecules and TJs (Supplementary Fig. 12a,b). Blocking or activating TREK1 did not alter cytokine production by human T cells stimulated with antibodies to CD3 and CD28 over 48 h (Supplementary Fig. 12c). TREK1 expression was reduced in endothelial cells in human multiple sclerosis lesions compared to normal-appearing white matter or healthy control samples (Fig. 4g and Supplementary Fig. 13a). This was associated with increased expression of ICAM1 and VCAM1 in CNS tissue from individuals with multiple sclerosis (Supplementary Fig. 13b–d).

In summary, our results suggest that an ion channel expressed by endothelial cells at the BBB regulates immune cell trafficking into the inflamed CNS. Further research efforts will be necessary to elucidate the detailed molecular pathways whereby this ion channel modulates BBB permeability. Possible mechanisms include both ion flux-dependent (for example, alterations in calcium concentrations) and ion flux-independent options (for example, interaction with the actin cytoskeleton¹⁸ or protein kinase pathways). As activation of TREK1 activity by ALA reduces EAE scores and lymphocyte infiltration into the CNS, these studies suggest that drugs targeted at modulating TREK1 activity may be used to treat various neurologic diseases associated with BBB damage.

METHODS

Methods and any associated references are available in the [online version of the paper](#).

Note: Any Supplementary Information and Source Data files are available in the [online version of the paper](#).

ACKNOWLEDGMENTS

This work was supported by the Deutsche Forschungsgemeinschaft (SFB TR128, TP B1 to H.W., SFB TR128, TP B6 to S.G.M., T.B. and H.-C.P.; SFB 1009, TP A3 to H.W.; FOR1086, TP2 to T.B. and S.G.M.; ME3283/2-1 to S.G.M.; and SFB688 TP A13 to C.K.), the Bundesministerium für Bildung und Forschung (Kompetenznetzwerk Multiple Sclerosis, 01GI0907 to H.W. and 01DJ12103 to T.B. and S.G.M.), the Else-Kröner-Fresenius Stiftung (C.K., S.G.M. and S.B.), the Interdisciplinary Center for Clinical Research (IZKF) Münster (SEED 03/12 to S.B.), the excellence cluster 'Cells in motion' (CIM, to S.G.M., H.W., S.B., T.B. and H.-C.P.), the CNRS and the LabEx Ionic channel Science and Therapeutics (M.B. and C.H.) and the Agence Nationale de la Recherche–ANR Emergence (ANR-11-EMMA to H.M.o.M.). We thank B. Reuter, E. Nass and J. Budde for excellent technical assistance and the UK Multiple Sclerosis Tissue Bank (R. Reynolds) for human brain tissue. The endothelial cell line bEND.5 was a kind gift from D. Vestweber (Max Planck Institute for Molecular Biomedicine).

AUTHOR CONTRIBUTIONS

S.B. and S.G.M. conceived the study and designed the experiments. S.B. and T.R. performed the main experimental work and analyzed the data. M.K.S., N.B., A.M.H., F.L., P.E., H.M.o.M., T.B. and K.G. performed additional experiments. M.B. and C.H. provided *Kcnk2*^{−/−} mice and spadin and supervised these experiments. D.S. and B.N. generated bone marrow chimeras. T.B., S.G.M. and H.-C.P. supervised the electrophysiological experiments and analyzed the data. H.-J.G. supervised the TER experiments. S.B. and T.R. drafted the manuscript, and C.K., H.W. and S.G.M. extensively revised the manuscript and funded the study. All authors provided input throughout the process.

COMPETING FINANCIAL INTERESTS

The authors declare no competing financial interests.

Reprints and permissions information is available online at <http://www.nature.com/reprints/index.html>.

1. Neuwelt, E.A. *et al.* Engaging neuroscience to advance translational research in brain barrier biology. *Nat. Rev. Neurosci.* **12**, 169–182 (2011).
2. Holman, D.W., Klein, R.S. & Ransohoff, R.M. The blood-brain barrier, chemokines and multiple sclerosis. *Biochim. Biophys. Acta* **1812**, 220–230 (2011).
3. Weiss, N., Miller, F., Cazaubon, S. & Couraud, P.O. The blood-brain barrier in brain homeostasis and neurological diseases. *Biochim. Biophys. Acta* **1788**, 842–857 (2009).
4. Overington, J.P., Al-Lazikani, B. & Hopkins, A.L. How many drug targets are there? *Nat. Rev. Drug Discov.* **5**, 993–996 (2006).
5. Honoré, E. The neuronal background K₂P channels: focus on TREK1. *Nat. Rev. Neurosci.* **8**, 251–261 (2007).
6. Heurteaux, C. *et al.* Deletion of the background potassium channel TREK-1 results in a depression-resistant phenotype. *Nat. Neurosci.* **9**, 1134–1141 (2006).
7. Alloui, A. *et al.* TREK-1, a K⁺ channel involved in polymodal pain perception. *EMBO J.* **25**, 2368–2376 (2006).
8. Heurteaux, C., Laigle, C., Blondeau, N., Jarretou, G. & Lazdunski, M. α -linolenic acid and riluzole treatment confer cerebral protection and improve survival after focal brain ischemia. *Neuroscience* **137**, 241–251 (2006).
9. Mazella, J. *et al.* Spadin, a sortilin-derived peptide, targeting rodent TREK-1 channels: a new concept in the antidepressant drug design. *PLoS Biol.* **8**, e1000355 (2010).
10. Wang, Q. & Doerschuk, C.M. The signaling pathways induced by neutrophil-endothelial cell adhesion. *Antioxid. Redox Signal.* **4**, 39–47 (2002).
11. Garry, A. *et al.* Altered acetylcholine, bradykinin and cutaneous pressure-induced vasodilation in mice lacking the TREK1 potassium channel: the endothelial link. *EMBO Rep.* **8**, 354–359 (2007).
12. Namiranian, K. *et al.* Cerebrovascular responses in mice deficient in the potassium channel, TREK-1. *Am. J. Physiol. Regul. Integr. Comp. Physiol.* **299**, R461–R469 (2010).
13. Duprat, F. *et al.* The neuroprotective agent riluzole activates the two P domain K⁺ channels TREK-1 and TRAAK. *Mol. Pharmacol.* **57**, 906–912 (2000).
14. Gilgun-Sherki, Y., Panet, H., Melamed, E. & Offen, D. Riluzole suppresses experimental autoimmune encephalomyelitis: implications for the treatment of multiple sclerosis. *Brain Res.* **989**, 196–204 (2003).
15. Nordøy, A. Dietary fatty acids and coronary heart disease. *Lipids* **34** (suppl.), S19–S22 (1999).
16. Lauritzen, I. *et al.* Polyunsaturated fatty acids are potent neuroprotectors. *EMBO J.* **19**, 1784–1793 (2000).
17. Nguemeni, C. *et al.* Dietary supplementation of α -linolenic acid in an enriched rapeseed oil diet protects from stroke. *Pharmacol. Res.* **61**, 226–233 (2010).
18. Lauritzen, I. *et al.* Cross-talk between the mechano-gated K₂P channel TREK-1 and the actin cytoskeleton. *EMBO Rep.* **6**, 642–648 (2005).

ONLINE METHODS

EAE experiments. All animal experiments were approved by local authorities and conducted according to the German law on animal protection (87-51.04.2012.A325). We induced EAE by immunization of 6- to 8-week-old female C57BL/6 (Charles River) or *Kcnk2*^{-/-} mice¹⁹ with MOG₃₅₋₅₅ peptide (Charité, Berlin, Germany). For the generation of bone marrow chimeras, we irradiated 5- to 6-week-old female WT and *Kcnk2*^{-/-} mice with a single dose of 10 Gy, and bone marrow cells from 6-week-old WT or *Kcnk2*^{-/-} mice from the same litter were injected intravenously into the irradiated mice (4×10^6 cells per mouse). Six weeks later, we injected MOG peptide, supplemented with complete Freund's adjuvant (CFA) to obtain a 1 mg ml⁻¹ emulsion, subcutaneously at the flanks of deeply anesthetized mice. Pertussis toxin was injected intraperitoneally on the day of immunization and then again 2 d later at a dose of 400 ng (Alexis). Two blinded observers monitored the clinical course of EAE using the following score system: 0, no abnormality; 1, limp tail tip; 2, limp tail; 3, moderate hindlimb weakness; 4, complete hindlimb paralysis; 5, mild paraparesis; 6, paraparesis; 7, paraplegia; 8, tetraparesis; 9, quadriplegia or premoribund state; 10, death.

For histologic evaluation of the mice with EAE, we removed the spinal cords and embedded them in optimal cutting temperature (OCT) compound Tissue-Tek (Sakura Finetek). Blocks were sectioned (10 μ m) in the transverse plane and stained with H&E or LFB according to standard protocols²⁰ or with antibodies to the following: ZO-1 (polyclonal, ab59720, Abcam), occludin (polyclonal, ab31721, Abcam), ICAM1 (YN1/1.7.4., ab119871, Abcam) or VCAM1 (324, ab78712, Abcam). Secondary antibodies were goat antibody to rat Cy3 (polyclonal, 112-165-008, Dianova) and goat antibody to rabbit Cy3 (polyclonal, 111-165-008, Dianova). All antibodies for flow cytometry were used at 1:100, and all antibodies for immunohistochemistry or western blotting were used at 1:200 dilution throughout the manuscript, if not stated otherwise. For quantification, we examined the staining under a microscope (Axiophot 2, Zeiss) equipped with a charge-coupled device (CCD) camera and analyzed it in a blinded manner using MetaVue Software (Molecular Devices).

Flow cytometry. CNS tissue from immunized mice at day 18 was dissociated mechanically, and mononuclear cells from the interface of a 30–50% Percoll (Amersham) density gradient centrifugation were counted by a Casy Model TT cell counter (Innovatis AG), stained with rat antibody to mouse CD4–peridinin chlorophyll (PerCP) (RM4-5, 553052), rat antibody to mouse CD8a–phycoerythrin (PE) (53-6.7, 553033) and rat antibody to mouse CD11b–allophycocyanin (APC) (M1/70, 553312) (all from BD Biosciences) following standard protocols. We then added Calibrite beads (BD Biosciences) and determined relative cell numbers by flow-assisted cell sorting (FACS-Calibur, BD Biosciences). In one set of experiments, we stained MBMECs and HBMECs with phalloidin-TRITC (Sigma-Aldrich) and analyzed them by flow cytometry.

Isolation of MBMECs. We prepared MBMECs from brains of naive and immunized WT and *Kcnk2*^{-/-} mice as described²¹ and used them for PCR analysis (see below). We controlled the purity by western blot analysis (see below) for the endothelial cell marker von Willebrand factor (vWF) and the immune cell marker CD2, as well as by immunocytochemical stainings of freshly prepared MBMECs for CD3 (KT3, MCA500GA, Serotec) and donkey antibody to rat Cy3 (polyclonal, 712-165-150, Dianova; **Supplementary Fig. 14a,b**). For functional analysis, we cultured cells 5 d before use on Transwell inserts coated with collagen IV and fibronectin (6.5 mm with a 3.0- μ m-pore polyester membrane insert; Corning Inc.) or 96-well flat-bottom plates (Nunc).

Culture of HBMECs. HBMECs (ScienCell Research Laboratories) were cultured in fibronectin-coated (2 μ g cm⁻²) T-75 flasks with microvascular endothelial cell growth medium (ScienCell Research Laboratories). We changed the medium every other day and split the cells from 90% confluence. Cells were harvested using accutase (PAA) according to the manufacturer's instructions, counted by a CASY Model TT cell counter (Innovatis AG) and used for further experiments.

TER measurements. We measured the TER of naive and *in vitro*-inflamed (IFN- γ and tumor necrosis factor- α (TNF- α), each 500 U ml⁻¹; Peprotech)

HBMEC or MBMEC layers for up to 7 d using a device for automated long-term monitoring (CellZscope). TER was assessed on endothelial cell monolayers cultured on 3.0- μ m-pore polyester membrane transwell inserts (Corning Inc.). We coated the transwell inserts with collagen IV (0.4 mg ml⁻¹) and fibronectin (0.1 mg ml⁻¹).

Transmigration assays. We performed transmigration assays with minor modifications as described^{22,23}. In brief, we assembled transwell inserts with HBMECs or MBMECs (1.5×10^5) as described above. Before transmigration, the naive and *in vitro*-inflamed (cultured with IFN- γ and TNF- α , each 500 U ml⁻¹, for 24 h) endothelial cell layers were treated with TREK1 modulators (as indicated in the figure legends) for 24 h. Afterwards we changed the cell culture medium and transferred human PBMCs or mouse splenocytes and CD4⁺ or CD8⁺ T cells (5×10^5 cells each) to the corresponding endothelial cell layer for 14 h. Migrated cells from the lower of the two compartments were collected, and Calibrite beads (BD Biosciences) were added^{22,24}. We used pretreatment with 100 μ M L-NAME for 8 h prior to cell transfer (Santa Cruz Biotechnology) in one set of experiments. Next we stained human cells with monoclonal antibodies to CD4 (RPA-T4, 300531, BioLegend), CD8 (RPA-T8, 301027, BioLegend), CD14 (M5E2, 301806, BioLegend), CD19 (HIB19, 555412, BD Biosciences) and CD56 (NCAM16.2, 341027, BD Biosciences) and mouse cells with antibodies to CD4 (GK1.5, 553730, BD Biosciences) and CD8 (53-6.7, 100712, BioLegend) and determined relative cell numbers by flow cytometry.

Cytokine detection and splenocyte proliferation. We quantified the production of IFN- γ , monocyte chemoattractant protein-1 (MCP-1), IL-8, interferon-inducible protein-10 (IP-10) and RANTES (also known as CCL5) in cultured PBMCs or HBMECs by a fluorescent bead immunoassay (FlowCytomix, Bender MedSystems) according to the manufacturer's instructions. Briefly, we stimulated PBMCs with CD3 and CD28 beads (1:10 bead-to-cell ratio; Dynabeads, Invitrogen). HBMECs were left untreated or incubated *in vitro* with IFN- γ and TNF- α (500 U ml⁻¹ each). Then we cultured cells for 24 h with modulators of TREK1 activity and analyzed the supernatants for the designated chemokines or cytokines by flow cytometry.

In one set of experiments, we stimulated splenocytes from naive or MOG-immunized mice with CD3 and CD28 beads or MOG peptide (10 μ g ml⁻¹) and assessed IFN- γ or IL-17 protein amounts by ELISA (R&D Systems). For assessment of cell proliferation, splenocytes were stimulated for 3 d after isolation with Dynabeads Human T-Activator CD3/CD28 (Invitrogen). [³H]-thymidine (1 μ Ci; Amersham) was added for the final 24 h. We measured radioactivity on a β -scintillation counter (TopCount NXT, PerkinElmer). In another set of experiments, we stimulated splenocytes with CD3 and CD28 beads for 3 d and assessed the amount of ATP in the supernatant after cell lysis, as a parameter of cell proliferation, using the ATP-Lite Luminescence Assay System (PerkinElmer) according to the manufacturer's instructions. Luminescence was measured on a BetaPlate Reader (Tecan). We performed all experiments in triplicate. ATP release assays and thymidine proliferation assays resulted in comparable results (**Fig. 1f** and **Supplementary Fig. 15**).

Western blot. We lysed cells in lysis buffer (1% NP-40, 1% n-dodecyl- β -D-maltoside, 1 mM sodium monovanadate, 1 mM PMSF, 50 mM Tris, 10 mM NaF, 10 mM EDTA and 165 mM NaCl) and incubated them on ice for 20 min. After centrifugation, the supernatant was mixed with 5 \times reducing sample buffer (0.1 M Tris, 50% glycerol, 5% sodium dodecyl sulfate, 0.25% bromophenolblue and 10% β -mercaptoethanol) and heated for 5 min to 99 $^{\circ}$ C. We separated the lysate on a denaturing and reducing 10% polyacrylamide gel and transferred the proteins to a nitrocellulose membrane. To detect the phosphorylation status of the signaling molecules, we incubated blots with phosphospecific antibodies to ERK (20G11, 4376), p38 (28B10, 9216), JNK (81E11, 4668) and AKT (C31E5E, 2965), all from Cell Signaling Technology, followed by incubation with peroxidase-conjugated secondary antibodies to rabbit or mouse IgG (Amersham, polyclonal, NA931 or NA934, 1:500). Alternatively, we used rabbit antibody to mouse TREK1 (polyclonal, T6448, Sigma-Aldrich), rabbit antibody to mouse vWF protein (H-300, sc-14014, Santa Cruz) and rabbit antibody to mouse CD2 (M-180, sc-28807, Santa Cruz). Bands were visualized using the enhanced

chemiluminescence (ECL) detection system (GE Healthcare). β -actin was used as a loading control.

RT-PCR. We isolated RNA from HBMECs and MBMECs following standard procedures. We performed cDNA synthesis using a standard protocol with random hexamer primers (Applied Biosystems) and ran RT-PCR with FAM-labeled TaqMan primers (all from Applied Biosystems) for TREK1 (Hs00247951_m1, Mm01323942_m1), TREK2 (Hs00368341_m1, Mm01335233_m1), TRESK (Hs00699272_m1, Mm01702237_m1), TRAAK (Hs00213267_m1, Mm00434626_m1), TASK1 (Hs00605529_m1, Mm00807036_m1), TASK2 (Hs00186652_m1, Mm00498900_m1), TASK3 (Hs00363153_m1, Mm02014295_s1), ICAM1 (Hs00164932_m1, Mm00516023_m1), VCAM1 (Mm01320970_m1), PECAM1 (Hs00169777_m1, Mm01242584_m1), occludin (Hs00170162_m1, Mm00500912_m1), claudin-5 (Hs00533949_s1, Mm00727012_s1) and ZO-1 (Hs00543824_m1, Mm00493699_m1), with VIC-labeled 18S rRNA as an endogenous control. We performed RT-PCR for 35 cycles and measured samples as triplicates. We calculated the data using the change in cycle threshold (Δ CT), $\Delta\Delta$ CT and relative quantification ($2^{-\Delta\Delta$ CT).

Brain tissue specimens. Human autopsy and biopsy materials from subjects with multiple sclerosis were received from the UK Multiple Sclerosis Tissue Bank (Division of Neuroscience and Mental Health, London, UK; $n = 5$ subjects). Studies on human samples were approved by the ethical board of the University of Münster. Informed consent was received from all patients. The lesions fulfilled the morphologic criteria of an inflammatory demyelinating process consistent with multiple sclerosis when stained with H&E, LFB and periodic acid Schiff (PAS), myelin stain and Bielschowsky's silver impregnation for axons. We classified lesions according to their demyelination status and included one early active, one late active and three inactive lesions. Staining was performed on 10- μ m coronal sections. For double labeling, slices were fixed in 4% paraformaldehyde (PFA) and incubated in blocking solution (5% BSA (PAA, Cölbe, Germany), 1% normal goat serum (NGS; PAA) and 0.2% Triton X-100 (Sigma-Aldrich, Munich, Germany). Afterwards we incubated the slices with antibodies to CD31 (WM-59, P8590, Sigma-Aldrich), TREK1 (polyclonal, T6448, Sigma-Aldrich), ICAM1 (HM.2, AM26247PU-N, Acris) or VCAM1 (1G11B1, AM26158PU-N, Acris). The secondary antibodies used were goat antibody to mouse Alexa Fluor 488 (polyclonal, A-11001, Invitrogen) and goat antibody to rabbit Cy3 (polyclonal, 111-165-008, Dianova).

DC-T cell coculture. For functional analysis, DCs from WT or *Kcnk2*^{-/-} mice were prepared from bone marrow cells flushed from femur and tibia bones as described previously²⁵. Bone marrow-derived DCs were harvested on day 9. The antibodies used for flow cytometric evaluation were to mouse CD11b-PerCP-Cy5.5 (M1/70, 550993), CD11c-APC (HL3, 550261), CD40-FITC (HM40-3, 553723), CD80-FITC (16-10A1, 553768) and CD86-FITC (GL1, 553691), all from BD Biosciences, and to MHC2-FITC (M5/114.15.2, 11-5321-81, eBioscience). For functional assessment, cells were incubated with 50 μ g ml⁻¹ MOG₃₅₋₅₅ for 6 h. Thereafter the MOG₃₅₋₅₅-loaded DCs were cocultured with magnetic-activated cell sorting (MACS)-isolated CD4⁺ T cells derived from immunized WT or *Kcnk2*^{-/-} mice at the maximum point of disease for 18 h, and supernatants were assessed for IFN- γ protein amounts by ELISA according to the manufacturer's instructions.

Electrophysiological measurements of endothelial cells. MBMECs and HBMECs were isolated and cultured as described above. All measurements were conducted in whole-cell configuration of the patch-clamp technique²⁶. Individual endothelial cells were identified by infrared differential interference contrast (DIC) microscopy²⁷. Whole-cell recording pipettes were fabricated from borosilicate glass (GT150T-10, Clark Electromedical Instruments; typical resistance, 5–8 M Ω) and filled with an intracellular solution containing (in mM): 95 K-gluconate; 20 K₃-citrate; 10 NaCl; 10 4-(2-hydroxyethyl)-1-piperazineethanesulfonic acid (HEPES); 1 MgCl₂; 0.5 CaCl₂; 3 BAPTA; 3 Mg-ATP; and 0.5 Na₂-GTP. The internal solution was set to a pH of 7.25 and an osmolality of 295 mOsm kg⁻¹. The extracellular solution contained (in mM): 120 NaCl; 2.5 KCl; 1.25 NaH₂PO₄; 30 HEPES; 2 MgSO₄; 2 CaCl₂; and

10 glucose; the external solution was set to a pH of 7.2, and the osmolality was set to 305 mOsm kg⁻¹. Membrane currents were recorded using an EPC-10 amplifier (HEKA Elektronik). Outward currents were elicited by repeated 500-ms rectangle pulses to 40 mV starting from a holding potential of -80 mV or by 200-ms ramps from -120 to +40 mV applied at 30-s intervals. A liquid junction potential of 16 mV was calculated using Clampex software and taken into account when analyzing the data.

Electrophysiological measurements of hTREK1 HEK cells. Human TREK1 HEK293 (hTREK1 HEK) cells were grown in the presence of 0.5 mg ml⁻¹ G418 in DMEM supplemented with 10% (vol/vol) heat-inactivated FBS containing 1% (vol/vol) penicillin and streptomycin in an atmosphere of 95% air and 5% CO₂ (ref. 28). Electrophysiological experiments were performed on hTREK1 HEK cells seeded at a density of 20,000 cells per 35-mm dish 2 d before testing. TREK1 current was recorded using the whole-cell configuration of the patch-clamp technique. Each current was calculated by using a RK 400 patch clamp amplifier (Axon Instruments), low-pass filtered at 3 kHz and digitized at 10 kHz using a 12-bit analog-to-digital converter digidata (1322 series, Axon Instruments). Patch-clamp pipettes were pulled using a vertical puller (PC-10, Narishige) from borosilicate glass capillaries and had a resistance of 3–5 M Ω . The bath solution contained (in mM) 150 NaCl, 5 KCl, 3 MgCl₂, 1 CaCl₂ and 10 HEPES adjusted to pH 7.4 with NaOH. The pipette solution contained (in mM) 155 KCl, 3 MgCl₂, 5 ethylene glycol tetraacetic acid (EGTA) and 10 HEPES adjusted to pH 7.2 with KOH. All experiments were performed at room temperature (21–22 °C). TREK1 currents were measured in the presence of a cocktail of potassium-channel inhibitors (K⁺ blockers: 3 mM 4-aminopyridine (4-AP), 10 mM tetraethylammonium (TEA), 10 μ M glibenclamide, 100 nM apamin and 50 nM charybdotoxin).

Stimulation protocols and data acquisition were carried out using a micro-computer (Dell Pentium) that used commercial software and hardware (pClamp 8.2). For pulse currents, cells were clamped at -80 mV, and voltage changes were applied by steps of 20 mV (from -100 mV to +60 mV). The duration of the depolarizing pulses was 825 ms, and the pulse cycling rate was 5 s. For ramp currents, cells were clamped at -80 mV, and voltage changes were applied by unique depolarization from -80 mV to +40 mV. The duration of the depolarization ramps was 500 ms, and the ramp cycling rate was 5 s. TREK1 current amplitudes were calculated at the end of the stimulation pulses. Cells were continuously superfused with a micropfusion system. Electrophysiological TREK1 current recordings were obtained using three channel activators, two fatty polyunsaturated acids (10 μ M AA and 10 μ M ALA), one benzothiazole (100 μ M riluzole)^{19,28,29} and one channel inhibitor (2 μ M spadin)^{9,30}. Current amplitudes were expressed as current densities. Results are expressed as the mean \pm s.e.m.

Potassium imaging. To assess intracellular K⁺ concentrations in cultured MBMECs, cells were loaded with Asante Potassium Green 1 (APG-1; TEFLabs), which is a fluorescent K⁺ indicator (through incubation with acetoxymethyl ester). A stock solution (2 mM) was prepared by dissolving APG-1 in DMSO containing 20% of the nonionic surfactant Pluronic F-127. Cells were incubated with 5 μ M of APG-1 in DMEM with 10% FBS for 70 min at room temperature. Cells were then transferred to an inverted microscope (Zeiss Axiovert 135) and viewed through a Zeiss \times 40 (1.4 numerical aperture (NA)) oil objective. Cells were maintained in a solution containing 145 mM N-methyl-D-glucamine chloride (NMDG), 10 mM HEPES, 3 mM KCl, 10 mM glucose, 1 mM CaCl₂ and 3 mM MgCl₂ (pH 7.35). The fluorescent probe was excited every 5 s by a 470-nm monochromatic light pulse (200 ms; VisiChrome, Visutron Systems) guided through an excitation band-pass filter (450–490 nm), a 510-nm dichroic mirror and a 520-nm-long pass filter. Fluorescence images were acquired with a cooled CCD camera (Cool Snap HQ, Photometrics). Background-corrected averaged fluorescence values were determined for cytoplasmic regions of interest using Metamorph software. To deplete cells of K⁺, 50 μ M gramicidin (an antibiotic compound that markedly increases membrane permeability to monovalent cations) was added to the extracellular solution. Increments of KCl (iso-osmolar exchange with NMDG-Cl) were added to raise potassium concentrations in the extracellular medium to various levels (5, 15, 45 or 145 mM). After each increment, as the intracellular and extracellular [K⁺] equilibrated,

a corresponding increase in intracellular indicator fluorescence was observed (Fig. 3a). The fluorescence intensity revealed a linear dependency ($r^2 > 0.981$) on the applied $[K^+]$. Extrapolation of cellular fluorescence before the application of gramicidin indicated that intracellular $[K^+]$ in WT (132 ± 1 mM (mean \pm s.e.m.), $n = 18$) and *Kcnk2*^{-/-} (131 ± 3 mM, $n = 10$) cells were not significantly ($P = 0.63$) different under native conditions.

DHE staining. The presence of ROS was visualized on frozen spinal cord sections using DHE staining. DHE is a cell-permeable compound that interacts with ROS to form oxyethidium, which in turn interacts with nucleic acids to emit a bright red color. Cryosections were incubated with 2 μ M DHE (2 mM stock solution dissolved in DMSO and diluted in PBS) for 30 min and washed with PBS. For staining of DNA, a fluorescent Hoechst dye (Hoechst 33342, Sigma-Aldrich) was added for 10 min at a concentration of 2 ng ml⁻¹. Sections were analyzed under a microscope (Nikon Eclipse 50i) equipped with a CCD camera, and fluorescence intensity was measured using the imaging software NIS-Elements.

Nitrotyrosine staining. Immunohistochemical staining for nitrotyrosine to visualize additional ROS was conducted on spinal cord sections. Cryo-embedded spinal cord slices were fixed in 4% PFA in PBS for 10 min and blocked for 1 h in 1% BSA in PBS to prevent nonspecific binding. A rabbit antibody to nitrotyrosine (polyclonal, 06-284, Upstate, dilution 1:100) was applied for 1 h in PBS containing 1% BSA. Proteins were detected by 45 min of incubation with Dylight 488-conjugated goat antibody to mouse secondary antibodies (polyclonal, ab96871, Abcam) at a dilution of 1:200 in 1% BSA in PBS. DNA was stained by adding 2 ng ml⁻¹ Hoechst (Hoechst 33342, Sigma-Aldrich) for 10 min. Sections were analyzed under a microscope (Nikon Eclipse 50i) equipped with a CCD camera.

Astrocyte experiments. Astrocyte cell cultures were obtained from C57BL/6 (WT) and *Kcnk2*^{-/-} postnatal day (P) 1–3 mice. Mice were killed by decapitation, their brains were transferred in Hanks' Balanced Salt Solution (HBSS), and the meninges were removed. After preparation of the cortex, tissue was collected in 13.5 ml HBSS and incubated for 15 min at 37 °C with 1.5 ml DNase I and 1.5 ml trypsin 2.5%. Cells were mechanically dissociated and filtered through a 45- μ m cell strainer. Then 4.5×10^6 astrocytes were cultured in 75-cm² flasks in astrocytes medium (1 \times minimum essential medium (MEM), 1 mM sodium pyruvate, 33.3 mM glucose, 10% horse serum and 1% penicillin and streptomycin). The medium was changed 24 h later and twice per week thereafter. When reaching a confluent layer, astrocytes were trypsinized with 0.25% trypsin and EDTA and frozen in freezing medium (astrocyte medium and 10% DMSO). Cells were defrosted and cultured on poly-D-lysine-coated cover slips for 2 weeks in astrocyte medium at 37 °C and 5% CO₂.

Astrocyte cultures were stained with the primary antibodies to the following: glial fibrillary acidic protein (GFAP) (G-A-5, G3893, Sigma-Aldrich, 1:400), glutamine synthetase (polyclonal, G2781, Sigma-Aldrich, 1:10,000), excitatory amino acid transporter 1 (EAAT1) (polyclonal, ab416, Abcam, 1:500) and the following secondary antibodies: goat antibody to mouse Alexa Fluor 488 (polyclonal, A-11001, Invitrogen) and goat antibody to rabbit Cy3 (polyclonal, 111-165-008, Dianova). Cell cultures were fixed with 4% PFA, washed with 10 mM PBS and incubated for 1 h at room temperature in 10 mM PBS containing 5% BSA, 1% goat serum and 0.3% Triton X-100 (Sigma). Primary antibodies were then diluted in 10 mM PBS containing 5% BSA and 1% goat serum and incubated for 1 h at room temperature. After washing steps with 10 mM PBS, secondary antibodies were diluted in 10 mM PBS containing 1% BSA. Astrocytes were then washed three times and covered with peqGOLD, and fluorescence was visualized as described above. In one set of experiments, cells were stimulated with IL-1 β and TNF- α , and IL-6 production in the supernatants were assessed by ELISA.

Determination of nitric oxide and ROS production. Nitric oxide was detected by staining with DAF-FM (Molecular Probes), and ROS were detected by staining the cells with CM-H2DCFDA (Molecular Probes). CM-H2DCFDA is oxidized to green fluorescent DCF (dichlorofluorescein) by H₂O₂. Cells were loaded with 10 μ M CM-H2DCFDA in HEPES ((in mM) 125 NaCl,

2.5 KCl, 1.25 NaH₂PO₄, 30 HEPES, 10 glucose, 2 MgSO₄ and 2 CaCl₂) for 40 min at 37 °C and 5% CO₂ and were then washed with HEPES. The MFI was determined as ROS generation using the TECAN Infinite M200PRO (TECAN Switzerland). Quantitative assessment of ROS generation was performed by normalization to the noninflamed control group.

Transwell permeability assay. Permeability across a confluent MBMEC monolayer was studied in a Coaster Transwell system (3.0- μ m pore size, 12 mm diameter; Corning Incorporated, Corning, NY). Permeability was assessed using two tracer molecules of different molecular sizes, Texas Red-labeled dextran (70 kDa) or fluorescein-labeled dextran (3 kDa) (25 μ g ml⁻¹, Invitrogen)³¹. The amount of tracer in the lower chamber was measured using a TECAN Infinite M200PRO (TECAN Switzerland).

BBB permeability *in vivo*. For analysis of BBB permeability at disease onset of EAE, 80 μ l of 2% Evans blue in PBS and 80 μ l of 25 mg ml⁻¹ Texas red-dextran or fluorescein-dextran in PBS were injected intravenously into the tail vein of immunized WT and *Kcnk2*^{-/-} mice. One or 24 h after injection, mice were perfused with PBS, and the brain and spinal cord were removed. Tissues were homogenized in N,N-dimethylformamide (for Evans blue) or 1% Triton-X100 in PBS (for dextran) and centrifuged 30 min at 16,000g. The supernatants were used for quantification with the TECAN Infinite M200PRO (TECAN, Switzerland) at 620 nm/680 nm (for Evans blue), 595 nm/615 nm (for Texas red-dextran) or 494 nm/521 nm (for fluorescein-dextran). Fluorescence from kidney tissue served as the positive control, and no significant differences were observed when values from CNS tissue were normalized to values from kidney tissue. Briefly, the amounts of tracer were determined from the formula $A_{620}/\text{wet weight (mg)}$ or $A_{540}/\text{wet weight (mg)}$.

Adoptive transfer EAE experiments. 2D2 mice containing MOG_{35–55}-specific T cells^{32,33} were crossed with *Kcnk2*^{-/-} mice. No increased frequency of spontaneous EAE development was observed in the 2D2 \times *Kcnk2*^{-/-} mice (data not shown). For adoptive transfer experiments, lymph node cells from 2D2 and 2D2 \times *Kcnk2*^{-/-} mice were stimulated *in vitro* in the presence of 10 μ g ml⁻¹ MOG_{35–55} peptide and 0.5 ng ml⁻¹ IL-12 for 3 d before i.p. transfer of 6×10^6 cells (using a protocol modified from ref. 34).

EAE experiments with treatment protocols. In one set of experiments, mice received riluzole (10 mg per kg body weight twice daily; Sigma-Aldrich, Munich, Germany) i.p. from the day of immunization or when the mice showed the first clinical signs of EAE. In another experiment, WT or *Kcnk2*^{-/-} mice received spadin (100 μ l, 10 μ M i.p. daily). In addition, two groups of mice were fed a diet enriched with 5% palmseed oil or linseed oil. Linseed oil contains ~70% PUFAs, mostly ALA (~55% of the total PUFAs), whereas palmseed oil is rich in saturated acids such as palmitic acid. The diet was started 2 weeks before immunization, and the pellets were renewed daily. The daily average food intake per mouse did not differ between the two groups (Supplementary Fig. 9a). In another set of experiments, blocking antibodies to VCAM1 (MECA367, BZL09353, Biozol) and ICAM1 (YN1/1.7.4, LS-C180069, Life Span Biosciences), each at 200 μ g, were applied intravenously at days 8 and 9 before clinical symptoms appeared, and analysis was performed 24 h later.

Statistical analyses. All results are presented as the mean \pm s.e.m. We performed statistical analyses using Student's *t* test³⁵ for normally distributed data or Mann-Whitney test for non-normally distributed data sets. We used one-way ANOVA with a Bonferroni *post-hoc* test for multiple comparisons. $P < 0.05$ was considered statistically significant.

- Heurteaux, C. *et al.* TREK-1, a K⁺ channel involved in neuroprotection and general anesthesia. *EMBO J.* **23**, 2684–2695 (2004).
- Bittner, S. *et al.* TASK1 modulates inflammation and neurodegeneration in autoimmune inflammation of the central nervous system. *Brain* **132**, 2501–2516 (2009).
- Schneider-Hohendorf, T. *et al.* Regulatory T cells exhibit enhanced migratory characteristics, a feature impaired in patients with multiple sclerosis. *Eur. J. Immunol.* **40**, 3581–3590 (2010).

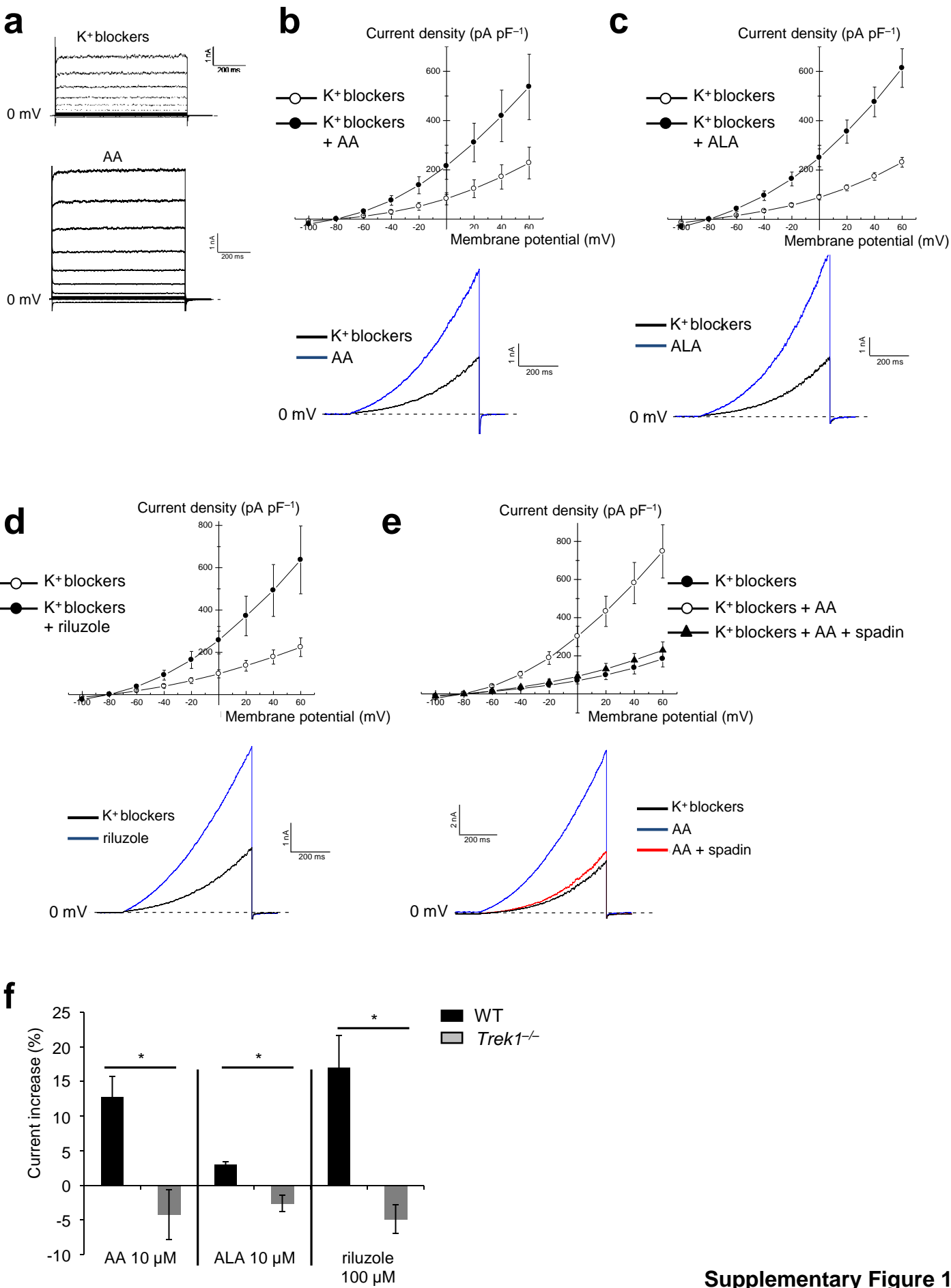


22. Göbel, K. *et al.* Blockade of the kinin receptor B1 protects from autoimmune CNS disease by reducing leukocyte trafficking. *J. Autoimmun.* **36**, 106–114 (2011).
23. Huang, Y.H. *et al.* Specific central nervous system recruitment of HLA-G⁺ regulatory T cells in multiple sclerosis. *Ann. Neurol.* **66**, 171–183 (2009).
24. Kleinewietfeld, M. *et al.* CCR6 expression defines regulatory effector/memory-like cells within the CD25⁺CD4⁺ T-cell subset. *Blood* **105**, 2877–2886 (2005).
25. Schuhmann, M.K. *et al.* Stromal interaction molecules 1 and 2 are key regulators of autoreactive T cell activation in murine autoimmune central nervous system inflammation. *J. Immunol.* **184**, 1536–1542 (2010).
26. Bittner, S. *et al.* Upregulation of K2P5.1 potassium channels in multiple sclerosis. *Ann. Neurol.* **68**, 58–69 (2010).
27. Dödt, H.U. & Ziegler-Schramm, W. Visualizing unstained neurons in living brain slices by infrared DIC-videomicroscopy. *Brain Res.* **537**, 333–336 (1990).
28. Moha ou Maati, H. *et al.* A human TREK-1/HEK cell line: a highly efficient screening tool for drug development in neurological diseases. *PLoS ONE* **6**, e25602 (2011).
29. Duprat, F. *et al.* The neuroprotective agent riluzole activates the two P-domain K⁺ channels TREK-1 and TRAAK. *Mol. Pharmacol.* **57**, 906–912 (2000).
30. Moha ou Maati, H. *et al.* Spadin as a new antidepressant: absence of TREK-1-related side effects. *Neuropharmacology* **62**, 278–288 (2011).
31. De Bock, M. *et al.* Low extracellular Ca²⁺ conditions induce an increase in brain endothelial permeability that involves intercellular Ca²⁺ waves. *Brain Res.* **1487**, 78–87 (2012).
32. Bettelli, E. *et al.* Myelin oligodendrocyte glycoprotein-specific T cell receptor transgenic mice develop spontaneous autoimmune optic neuritis. *J. Exp. Med.* **197**, 1073–1081 (2003).
33. Krishnamoorthy, G., Holz, A. & Wekerle, H. Experimental models of spontaneous autoimmune disease in the central nervous system. *J. Mol. Med. (Berl)* **85**, 1161–1173 (2007).
34. Williams, J.L. *et al.* Memory cells specific for myelin oligodendrocyte glycoprotein (MOG) govern the transfer of experimental autoimmune encephalomyelitis. *J. Neuroimmunol.* **234**, 84–92 (2011).
35. Dixon, W. & Massey, F. *Introduction to Statistical Analysis* (McGraw-Hill Companies, New York, 1969).

Endothelial TWIK-related potassium channel-1 is a critical regulator of immune cell trafficking into the CNS

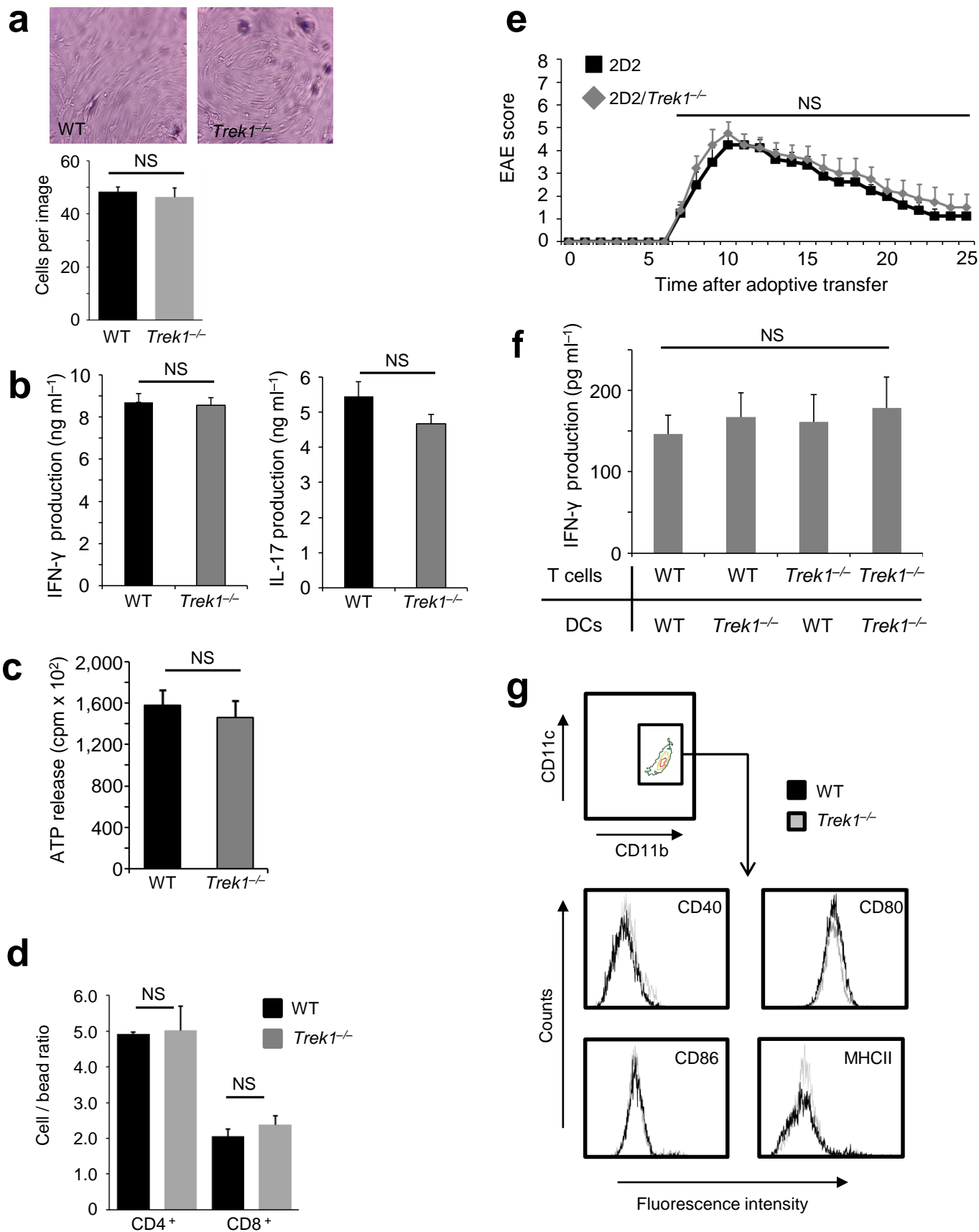
Stefan Bittner, Tobias Ruck, Michael K Schuhmann, Alexander M Herrmann, Hamid Moha ou Maati, Nicole Bobak, Kerstin Göbel, Friederike Langhauser, David Stegner, Petra Ehling, Marc Borsotto, Hans-Christian Pape, Bernhard Nieswandt, Christoph Kleinschnitz, Catherine Heurteaux, Hans-Joachim Galla, Thomas Budde, Heinz Wiendl & Sven G. Meuth

Supplementary Information

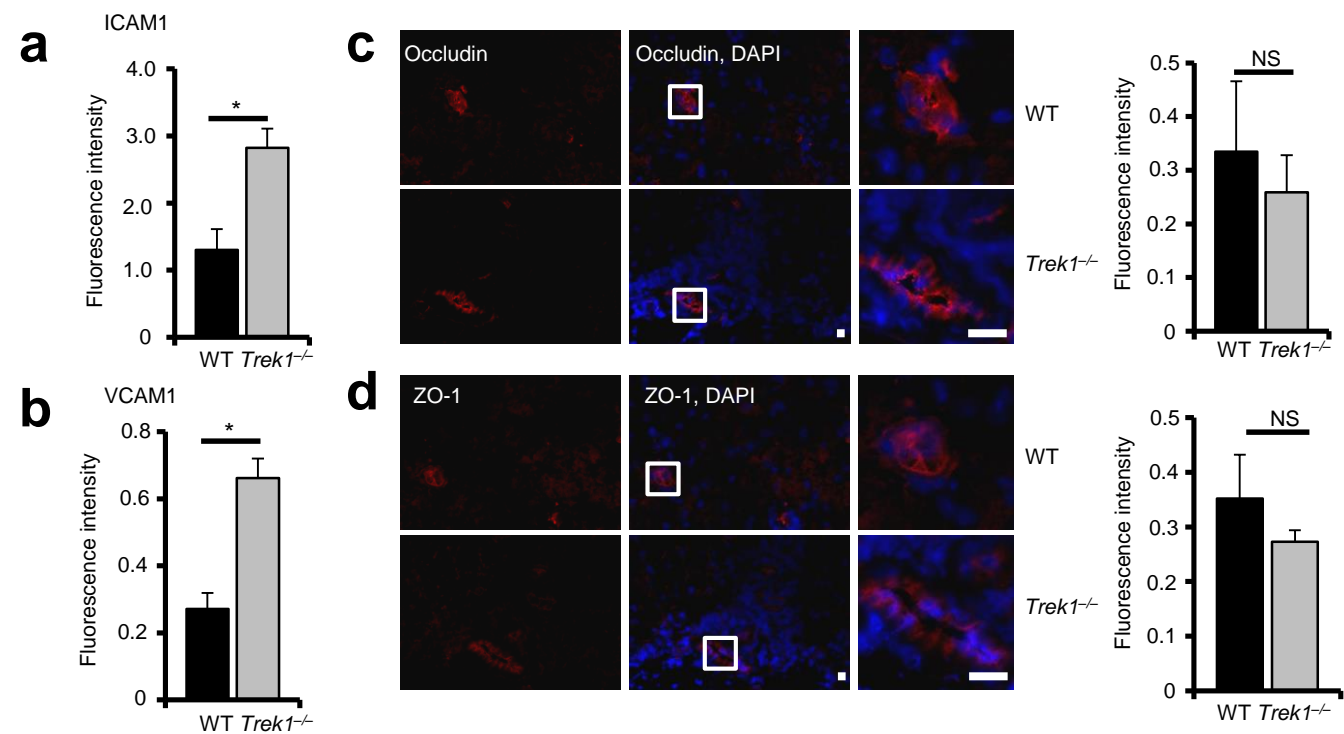


Supplementary Figure 1

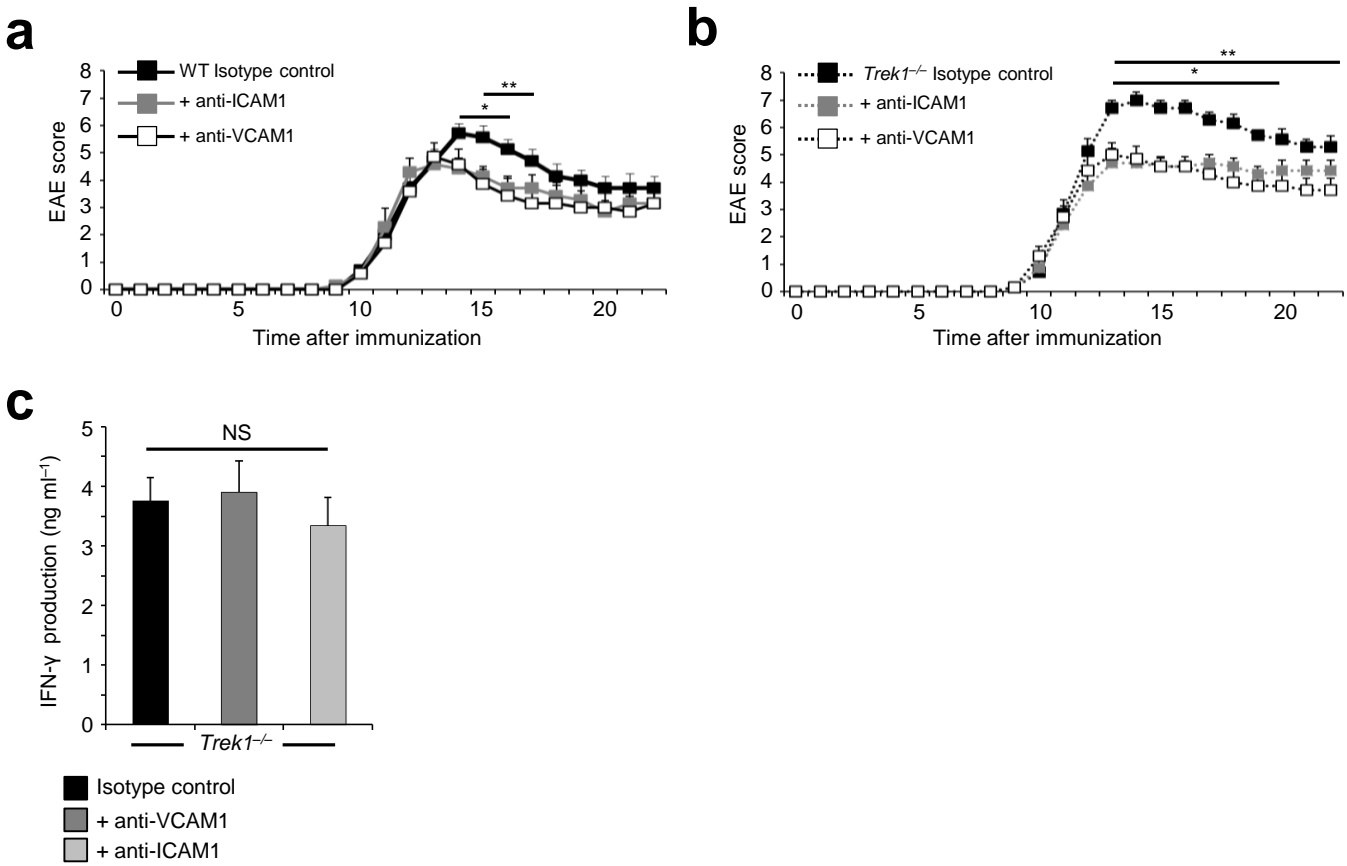
Supplementary Figure 1 Electrophysiological characterization of human TREK1/HEK (hTREK1/HEK) cells and mouse brain microvascular endothelial cells (MBMEC). (a) Pharmacological activation of hTREK1 currents with 10 μ M arachidonic acid (AA) in whole-cell patch-clamp configuration on a hTREK1/HEK cell line. Currents were recorded in the presence of a cocktail of potassium channel inhibitors (K^+ blockers). Representative current traces are shown. (b) Current-voltage relationship curves obtained before (open circles) and after (closed circles) current activation by AA 10 μ M ($n = 10$). Lower panel: Typical ramp traces obtained in control conditions and in the presence of 10 μ M AA. (c) Current-voltage relationships obtained before (open circles) and after (closed circles) current activation by alpha-linolenic acid (ALA) 10 μ M ($n = 10$). Lower panel: Typical ramp traces obtained in control conditions and in the presence of 10 μ M ALA. (d) Current-voltage relationships obtained before (open circles) and after (closed circles) current activation by riluzole 100 μ M ($n = 10$). Lower panel: Typical ramp traces obtained in control conditions and in the presence of 100 μ M riluzole. (e) After the pre-activation of the current by 10 μ M AA, the inhibition of the current by 2 μ M of spadin was measured. Current-voltage relationships obtained in the presence of K^+ blockers (closed circles), K^+ blockers + AA (open circles) and K^+ blockers + AA + spadin 2 μ M (closed triangles). Lower panel: Typical ramp traces obtained in the presence of K^+ blockers (black line), K^+ blockers + AA (blue line) and K^+ blockers + AA + spadin 2 μ M (red line). (f) Application of AA, ALA and riluzole on MBMEC from wild type (WT) and *Trek1*^{-/-} mice ($n = 5$, respectively). Relative current change is shown. * $p < 0.05$.



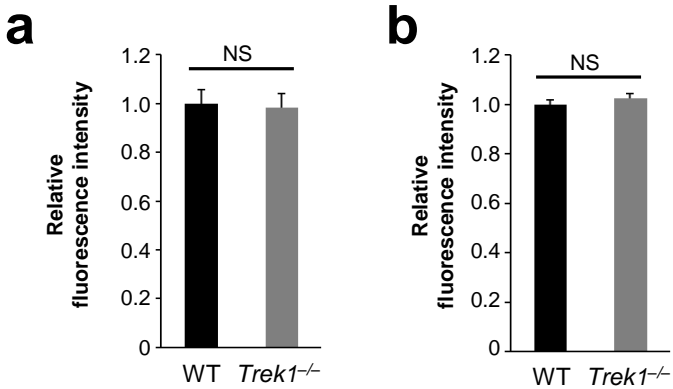
Supplementary Figure 2 MBEMC, lymphocytes and dendritic cells from *Trek1*^{-/-} and WT mice exhibit a comparable immunological profile. **(a)** MBMEC cell layers prepared from WT or *Trek1*^{-/-} mice displayed similar densities. Representative images of MBMEC layers are shown with cell densities (number of cells per image) expressed in the bar chart. **(b,c)** WT and *Trek1*^{-/-} splenocytes showed comparable levels of IFN- γ and IL-17 production **(b)** and similar proliferation rates **(c)** after stimulation with CD3/CD28 beads. **(d)** Migratory capacity of WT and *Trek1*^{-/-} CD4⁺ and CD8⁺ T cells across transwell filters devoid of ECs ($n = 5$). **(e)** Adoptive transfer EAE scores in WT recipients of *in vitro* stimulated 2D2 or 2D2/*Trek1*^{-/-} cells ($n = 8$ vs 7). **(f)** Co-culture experiment of dendritic cells (DCs) and T cells from immunized WT ($n = 5$) and *Trek1*^{-/-} mice ($n = 5$) isolated at disease maximum and vice versa. Co-cultures were assessed for IFN γ production after MOG stimulation. **(g)** Characterization of CD11b⁺CD11c⁺ antigen presenting cells in WT and *Trek1*^{-/-} mice by flow cytometry for the surface markers MHCII, CD80, CD86 and CD40. No significant differences were observed ($n = 5$). ns = not significant.



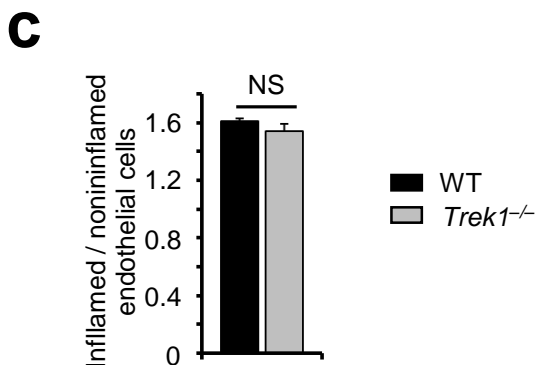
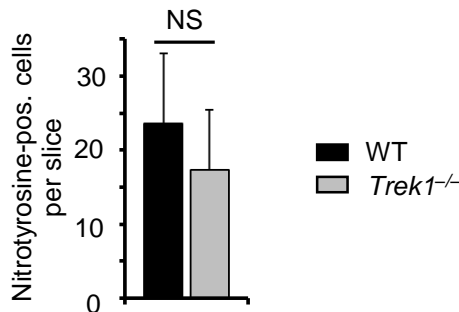
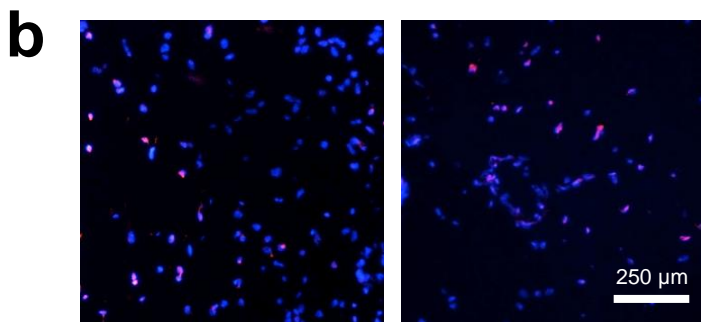
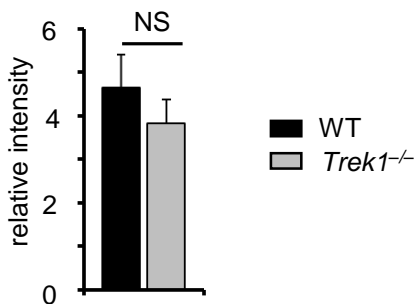
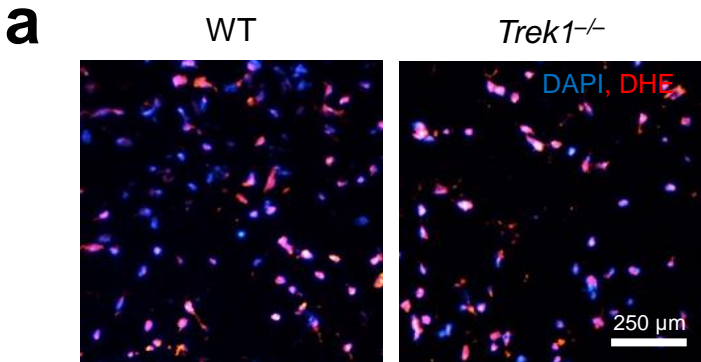
Supplementary Figure 3 An upregulation of ICAM1 and VCAM1 but no changes for Occludin and ZO-1 can be observed in EAE lesions from *Trek1*^{-/-} mice compared to WT mice. **(a,b)** Fluorescence intensity of **(a)** ICAM1 and **(b)** VCAM1 expression in EAE lesions from WT and *Trek1*^{-/-} mice ($n = 5$, $p < 0.5$). Representative results are also displayed in **Fig. 2c,d**. **(c,d)** Representative results and evaluation for **(c)** Occludin and **(d)** ZO-1 expression in EAE lesions from WT and *Trek1*^{-/-} mice ($n = 5$). ns = not significant.



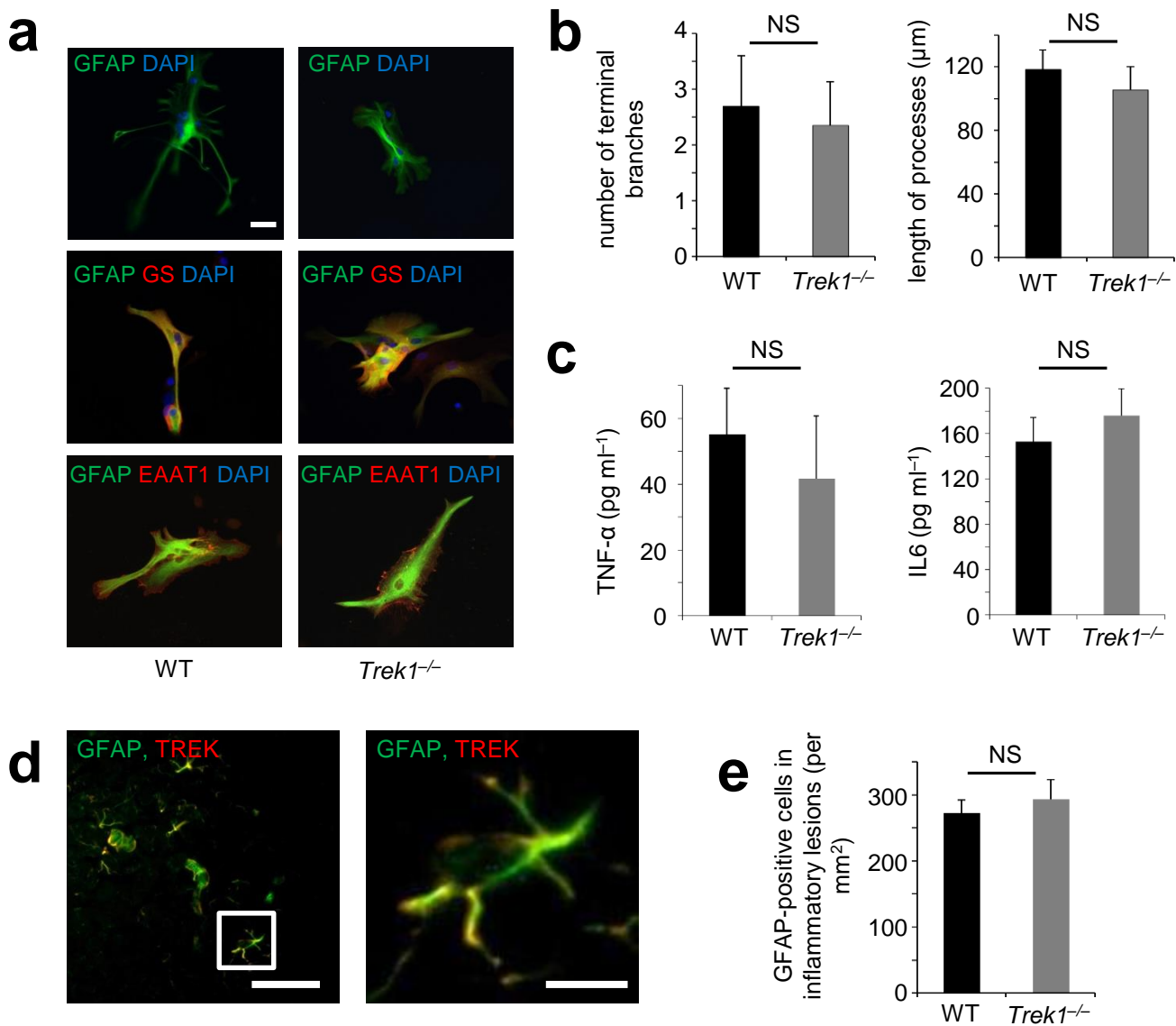
Supplementary Figure 4 EAE course and evaluation of anti-ICAM1 and anti-VCAM1 treated WT and *Trek1*^{-/-} mice. **(a,b)** EAE course in **(a)** WT and **(b)** *Trek1*^{-/-} mice receiving blocking antibodies against VCAM1 or ICAM1 or isotype controls on day 8 and day 9 (*n* = 8 per group). **(c)** ELISAs for IFN- γ in isotype- or antibody-treated *Trek1*^{-/-} splenocytes at disease maximum.



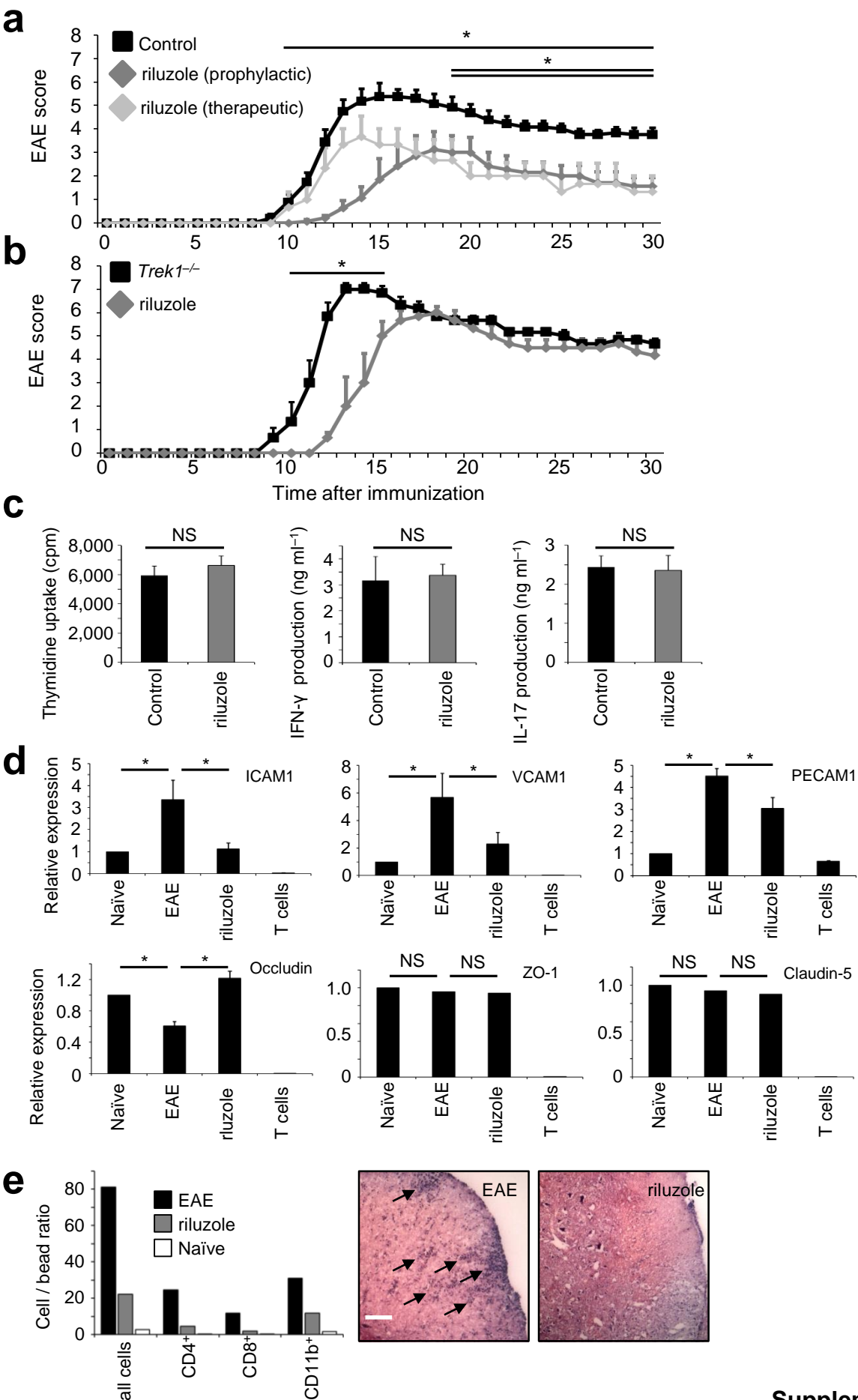
Supplementary Figure 5 *Trek1* deletion has no impact on the permeability of MBMEC for molecular tracers *in vitro*. (**a,b**) No significant difference was found for permeability for (**a**) Dextran 3 kDa-Fluorescein and (**b**) Dextran 70 kDa-TR over 10 minutes ($n = 6$, respectively). Later time points up to 12 hours also revealed no significant differences (data not shown).



Supplementary Figure 6 Reactive oxygen species/reactive nitrogen species (ROS/RNS) production is unchanged upon *Trek1* deletion in endothelial cells. **(a,b)** EAE lesions in WT and *Trek1*^{-/-} were characterized by H&E and LFB staining (not shown) and further characterized by staining for DHE **(a)** and nitrotyrosine **(b)**. Representative pictures are displayed on the left side and evaluation on the right side. Scale bar = 250 μm. **(c)** *In vitro* assessment of ROS production in MBMEC revealed no differences between WT and *Trek1*^{-/-} mice (n=5). DAPI = 4',6-diamidino-2-phenylindole; ns = not significant.

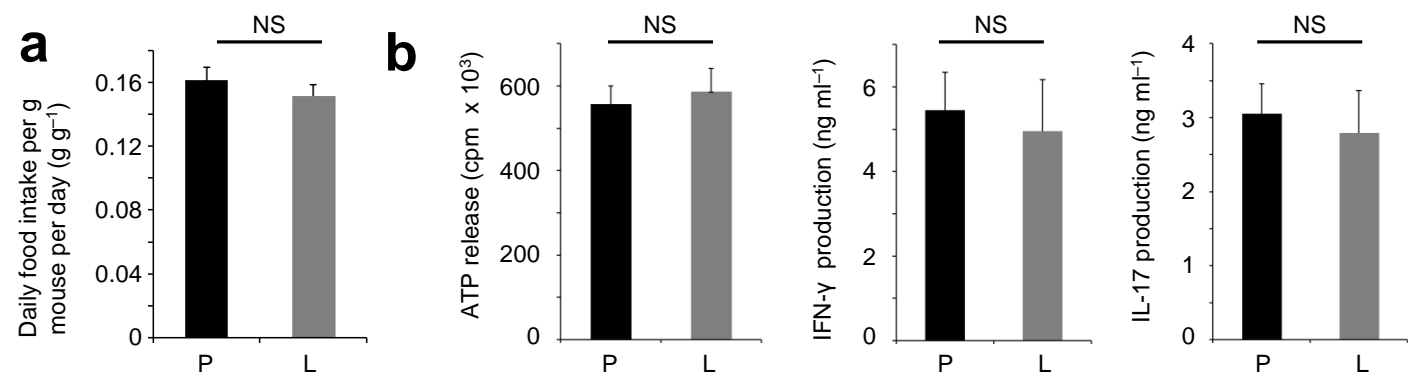


Supplementary Figure 7 *Trek1* deletion has no impact on astrocyte morphology and function. **(a)** Histologic staining of cultured astrocytes for glial fibrillary acidic protein (GFAP), glutamine synthetase (GS), and excitatory amino acid transporter 1 (EAAT1) revealed comparable results. **(b)** Morphologic analysis of astrocytes showed no differences in the number of terminal branches and the lengths of cell processes. **(c)** Stimulation of cultured astrocytes with IL-1 β resulted in a comparable production of TNF- α and IL-6. **(d)** Representative GFAP staining of TREK1-expressing astrocytes in EAE lesions from immunized WT mice. **(e)** Quantification of astrocyte numbers in EAE lesions of WT and *Trek1*^{-/-} mice showed a similar number of GFAP-positive cells. ns = not significant.

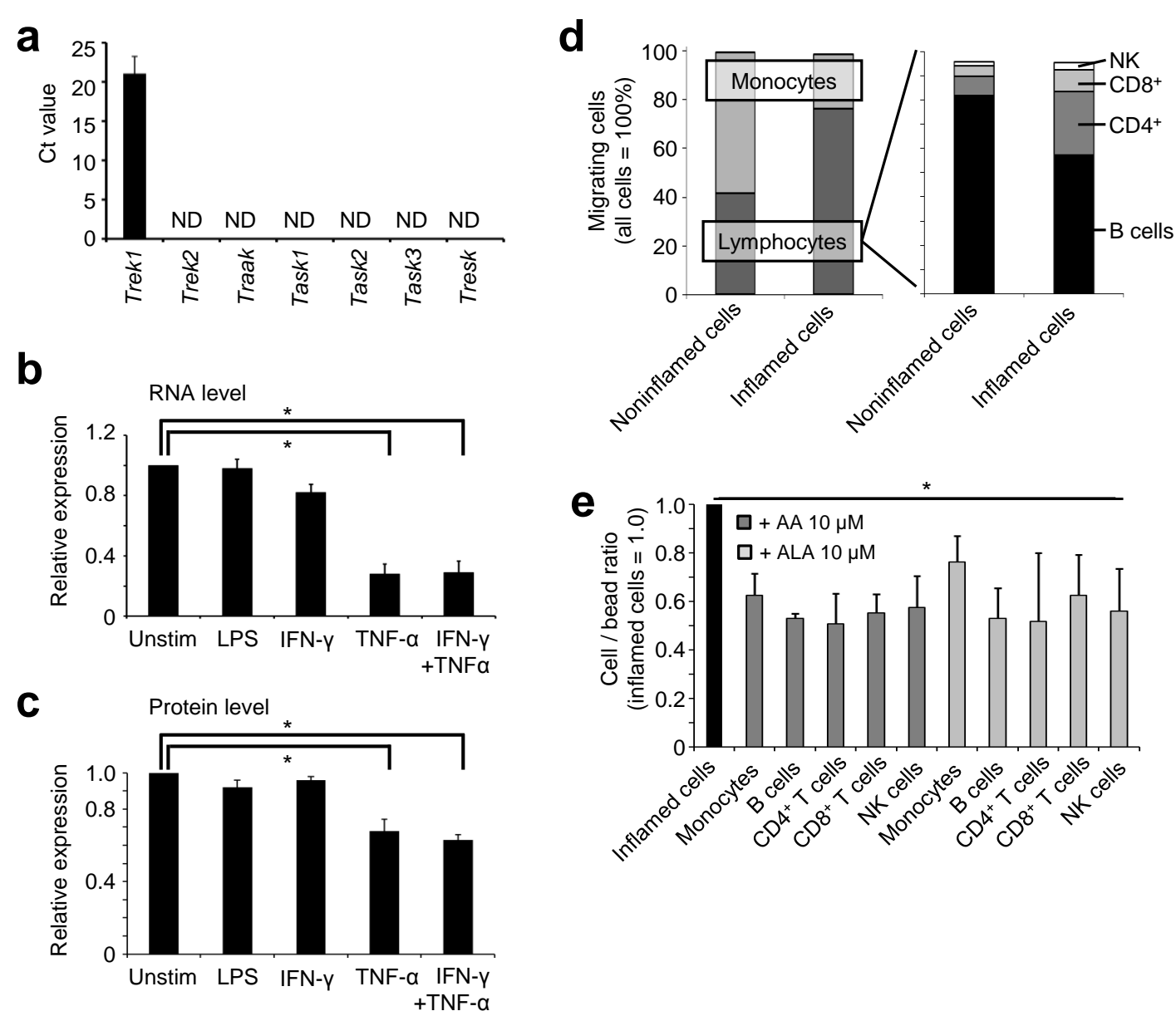


Supplementary Figure 8

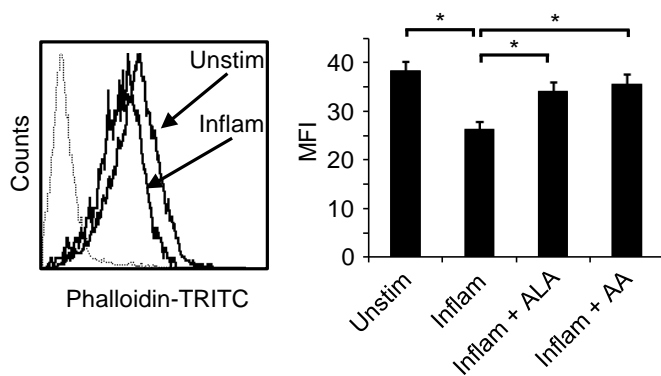
Supplementary Figure 8 TREK1 activation reduces immune cell trafficking *in vivo* and ameliorates the disease course of EAE. **(a)** The TREK1 activator riluzole (10 mg/kg, twice daily) significantly ameliorated the course of EAE when administered prophylactically (starting from the day of immunization) or therapeutically (starting after the first signs of EAE) compared with untreated mice (single horizontal line: control versus riluzole (prophylactic); double horizontal line: control versus riluzole (therapeutic); $n = 10$ mice per group). **(b)** Riluzole administration in *Trek1*^{-/-} mice resulted in a significantly delayed disease onset, while it had no influence on the EAE course beyond day 15 ($n = 10$ mice per group). **(c)** Proliferation rate and cytokine production of splenocytes isolated from riluzole-treated or untreated mice at maximum extent of EAE showed no significant (ns) differences. **(d)** MBMEC from naïve mice were compared with MBMEC isolated at the maximum extent of EAE from immunized untreated mice and riluzole-treated mice for the expression of EC markers. T cells served as negative controls. **(e)** Flow cytometry assessment of CNS-invading cells (left panel; one representative example out of three) and representative histologic staining of inflammatory foci in the spinal cord (H&E stain, black arrows). $*P < 0.05$; Scale bar represents 100 μM . ICAM1 = intercellular adhesion molecule 1; IFN- γ = interferon- γ ; IL-17 = interleukin-17; PECAM1 = platelet endothelial cell adhesion molecule 1; VECAM1 = vascular cell adhesion molecule 1. $*p < 0.05$.



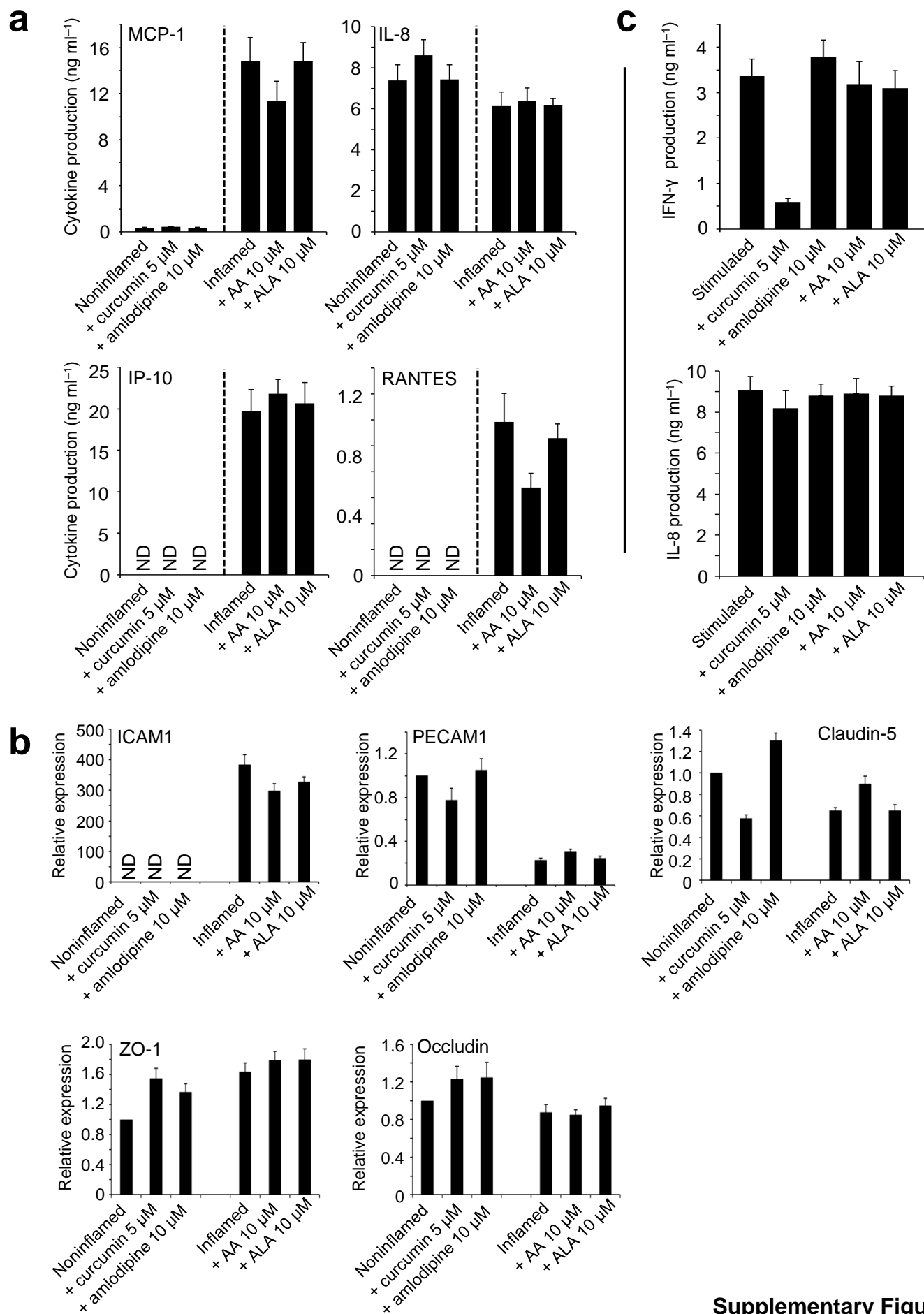
Supplementary Figure 9 Evaluation of dietary enrichment with linseed oil or palmseed oil for treated EAE animals with regard to food intake and T cell effector function. **(a)** Daily food intake per mouse per day was unchanged in the palm seed oil (P) and linseed oil (L) group. **(b)**. Splenocytes isolated at disease maximum showed a comparable proliferation rate (left panel) and IFN- γ - and IL-17-production (middle and right panels, respectively) upon MOG restimulation. ns = not significant.



Supplementary Figure 10 Characterization of HBMEC *in vitro*. **(a)** Gene expression of different K_{2P} channels in HBMEC ($n = 5$). **(b)** *Trek1* gene expression in HBMEC under different inflammatory stimuli, normalized to unstimulated (Unstim) cells ($n = 5$ per group). **(c)** TREK1 protein expression in HBMEC under different inflammatory stimuli. The densitometric quantification is shown ($n = 5$ per group). **(d)** Relative migration of monocytes and lymphocytes under non-inflamed and inflamed conditions. Lymphocytes are further divided into subtypes. **(e)** The TREK1 activators arachidonic acid (AA) and alpha-linolenic acid (ALA) cause a comparable reduction of immune cell migration *in vitro*. LPS = lipopolysaccharide; nd = not detectable; NK = natural killer. * $p < 0.05$.

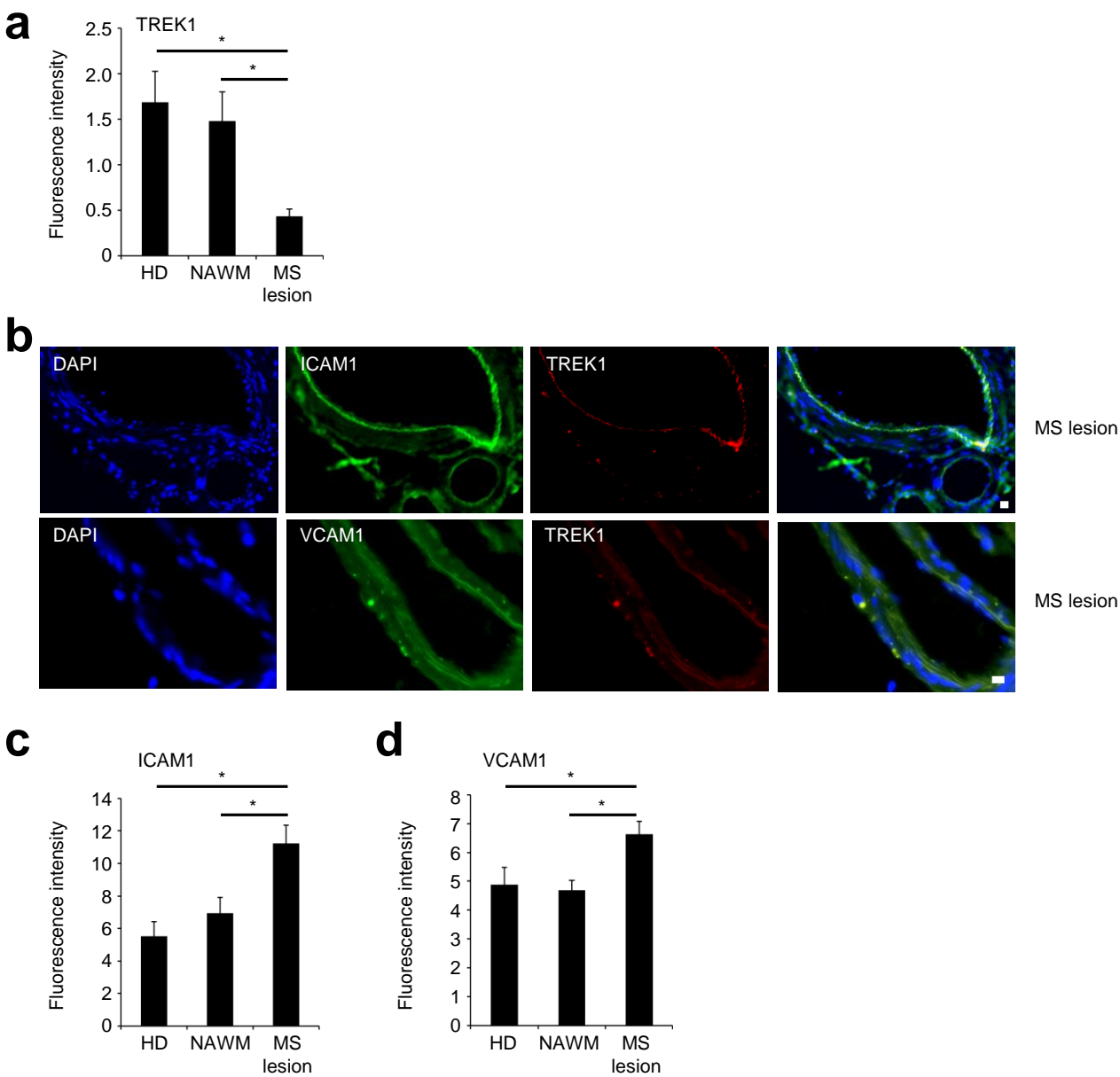


Supplementary Figure 11 Reduction of actin polymerization under inflammatory conditions is restored by TREK1 activation. The measurement of F-actin content of HBMEC stained with phalloidin-TRITC using flow cytometry is shown in the histogram and quantified in the bar chart. Unstim = unstimulated; Inflam = inflamed; ALA = linolenic acid; AA = arachidonic acid. * $P < 0.05$.

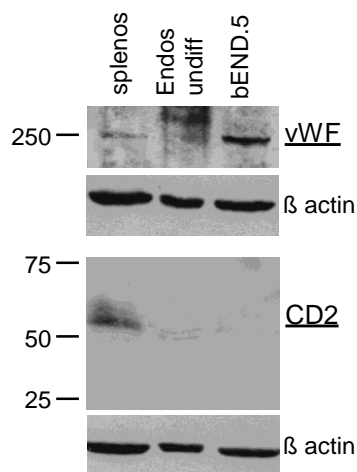
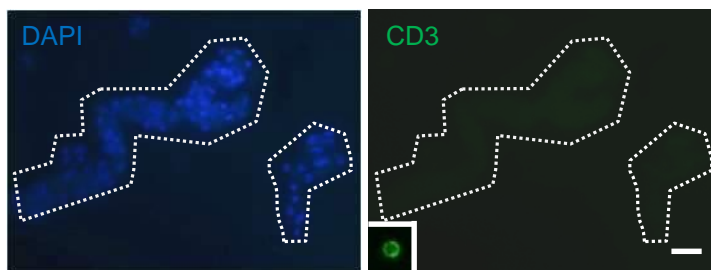


Supplementary Figure 12

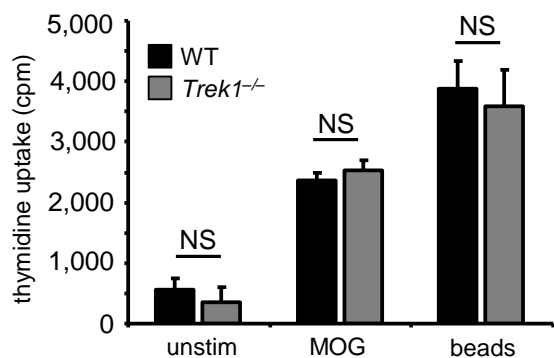
Supplementary Figure 12 TREK1 modulation has no influence on the cytokine profile of HBMEC and PBMC or on EC markers. **(a)** TREK1 modulation did not affect the secretion of MCP-1, IL-8, IP-10 and RANTES by HBMEC. **(b)** Expression of ICAM1, PECAM1, claudin-5, ZO-1 and occludin was not altered by TREK1 modulation. **(c)** The cytokine profile of T cells was not changed by TREK1 modulation. AA = arachidonic acid, ALA = alpha-linolenic acid. $n = 5$; ns = not significant.



Supplementary Figure 13 TREK1 downregulation is associated with ICAM1 and VCAM1 upregulation in human MS lesions. **(a)** Fluorescence intensity of TREK1 expression in CNS tissue of healthy control subjects (HD) and normal appearing white matter (NAWM) and lesions of MS subjects (MS lesion; $n = 5$, respectively). Representative pictures are depicted in **Fig. 4g**. **(b)** Immunohistochemical costaining for ICAM1, VCAM1 and TREK1 in MS lesions (representative results). **(c,d)** Fluorescence intensity of **(c)** ICAM1 and **(d)** VCAM1 expression ($n = 4$).

a**b**

Supplementary Figure 14 Purity controls after MBMEC preparation. **(a)** Western blot analysis from freshly isolated splenocytes, freshly isolated MBMEC (Endos undiff) and from the endothelial cell line bEND.5 for the brain endothelial cell marker von Willebrand factor (vWF) and the immune cell marker CD2. Purity controls were performed on a regular basis and one representative example is shown. **(b)** Immunocytochemical staining of freshly isolated MBMEC from immunized WT mice at disease maximum for CD3 (left: DAPI; right: CD3). Inset shows a staining of a splenocyte for visual comparison in the same scale). Scale bar represents 20 μ m.



Supplementary Figure 15 Comparison of proliferation assays. Thymidine-uptake assays and ATP release assays showed comparable results as depicted in **Figure 1f**.